To the Graduate Council:

I am submitting herewith a thesis written by Andrew Stewart Fleming entitled "The Effects of Piston Stroke Length and Exit Geometry on the Kinematics of Vortex Rings." I have examined the final copy of this thesis for form and content and recommend that it be accepted in partial fulfillment of the requirements for the degree of Master of Science, with a major in Aerospace Engineering.

Ahmad D. Vakili, Major Professor

We have read this thesis
and recommend its acceptance:

John E. Cartwright

Accepted for the Council:

Associate Vice Chancellor
and Dean of the Graduate School

STATEMENT OF PERMISSION TO USE

In presenting this thesis in partial fulfillment of the requirements for a Master's degree at the University of Tennessee, Knoxville, I agree that the library shall make it available to borrowers under the rules of the library. Brief quotations from this thesis are allowable without special permission, provided that accurate acknowledgment of the source is made.

Permission for extensive quotation from or reproduction of this thesis may be granted by my major professor, or in his absence, by the Head of Interlibrary Services when, in the opinion of either, the proposed use of the material is for scholarly purposes. Any copying or use of the material in this thesis for financial gain shall not be allowed without my written permission.

Signature Andrew Fleming

Date 19 Aug 92

THE EFFECTS OF PISTON STROKE LENGTH AND EXIT GEOMETRY ON THE KINEMATICS OF VORTEX RINGS

A Thesis
Presented for the
Master of Science
Degree
The University of Tennessee, Knoxville

Andrew Stewart Fleming
December 1992

ACKNOWLEDGEMENTS

I have been deeply impressed with the atmosphere of co-operation and concern which I have found at the University of Tennessee Space Institute. My development has benefited greatly from contact with faculty and students who have a keen interest in learning and a willingness to share their knowledge.

I am indebted to fellow students for helping me to open previously locked doors and for showing me that you can always push yourself harder. I would like to thank Jim Boazman, Ricky Meeker, Dick Ray, and Harold Sartain for their practical help and common sense in the laboratory. Finally, special thanks are accorded to my adviser Dr. Ahmad Vakili for his guidance and understanding throughout my two years here.

ABSTRACT

This investigation looked at the relationships between the piston stroke length and the exit geometry of a vortex generator and the dependent characteristics of a vortex ring. The vortex generator was operated with two exit geometries, one a conventional straight tube and the other a sharp edged orifice with the same exit diameter as the straight tube. Rings were generated in the University of Tennessee Space Institute water tunnel in order to facilitate the study of ring characteristics in both a quiescent fluid and in the presence of a uniform cross flow.

Quantitative measurements were taken using hot film anemometry and qualitative observations were made using flow visualization techniques. Experimental results indicated that within the range of parameters used for these experiments, ring circulation and diameter increased with increasing stroke length. Additionally, the diameter of highly turbulent rings generated with the sharp edged exit increased slowly during the initial stage of ring motion. This was then followed by a rapid increase in ring growth. In addition, the sharp edged rings had larger cores and smaller overall diameters, and shed more of their initial vorticity into their wakes than the straight tube rings. Finally, tests yielded conclusive evidence of the tilting of vortex rings in the presence of a cross flow.

TABLE OF CONTENTS

		Page
I.	INTRODUCTION	1
II.	TECHNICAL REVIEW	2
	Initial Vortex Ring Characteristics	4
	Circulation	6
	Ring Diameter	10
	Core Diameter	13
	Translational Velocity	13
	Vortex Ring Kinematics	14
	Laminar Vortex Ring	15
	Transition	16
	Turbulent Vortex Ring	18
	Viscous Vortex Ring Model	19
	Translating Vortex Ring in a Cross Flow	20
	Summary	20
III.	EXPERIMENTAL PROCEDURE	22
	Water Tunnel	22
	Vortex Generator	22
	Piston Velocity Profiles	26
	Hot Film Anemometer Measurements	30
	Calibration of Probe	30
	Directional Sensitivity of Probe	31
	Mean Velocity Components	36
	Fluctuation in the Measurement of Cross Flow Velocity	36
	Vortex Ring Velocity Measurements	37
	Flow Visualization	37
	Evaluation of Characteristic Parameters	39
	Circulation	39
	Ring Diameter	40

Core Diameter 41
Translational Velocity 41

IV. EXPERIMENTAL RESULTS AND ANALYSIS 42
Circulation 42
Ring Diameter 49
Entrainment 51
Core Diameter 55
Translational Velocity 55
Accuracy of Experimental Results 57

V. CONCLUSIONS AND RECOMMENDATIONS 59

LIST OF REFERENCES 62

APPENDICES 64
Appendix A 65
Appendix B 66

VITA 67

LIST OF FIGURES

Figure		Page
2.1.	Roll up of vortex ring (a) Initial flattening (b) Roll up	3
2.2.	Piston-cylinder configurations (a) Straight tube configuration (b) Sharp edged configuration	5
2.3.	Sketch of velocity profiles in exit plane of nozzle used for Didden's (3) experiments	9
2.4.	Production of vorticity during roll up (a) Straight tube configuration (b) Sharp edged configuration	11
2.5.	Stationary wave core instability during transition	17
2.6.	Tilting of vortex ring in cross flow	21
3.1.	Water tunnel test section	23
3.2.	Vortex generator system	24
3.3	Piston velocity profiles of test configurations used for the analysis of circulation (a) Piston stroke length 0.8 inches	27
	(b) Piston stroke length 0.5 inches	28
	(c) Piston stroke length 0.25 inches	29

3.4. Anemometer calibration channel 32

3.5. Typical calibration curve for hot film probe 33

3.6. Pitch and yaw angles relative to probe 34

3.7. Vortex ring velocity measurements 38

4.1. Hot film anemometer voltage-time histories
(a) Voltage-time history showing centre of core passing by probe 43
(b) Voltage-time history showing inner edge of core passing by probe 44

4.2. Ratio of measured to initial circulation versus Reynolds number 47

4.3. Measurement of vortex ring tilt angle 48

4.4. Vortex ring tilting in a uniform cross flow
(a) Straight tube - 0.25 inch stroke with 35 psi and $U_e/U_\infty = 9.2$
(b) Straight tube - 0.25 inch stroke with 25 psi and $U_e/U_\infty = 4.3$ 50

4.5. Flow visualization results of entrainment process
(a) Fluid emerging from the cylinder
(b) Fluid 1 to 2 D_e from the exit 52

4.6. Flow visualization of straight tube vortex ring entrainment properties 54

4.7. Flow visualization of sharp edged vortex ring entrainment properties
(a) 25 psi test
(b) 45 psi test 56

LIST OF TABLES

Table		Page
2.1.	Classification of flow regimes	14
4.1.	Initial and measured ring circulation	46
4.2.	Uncertainties in hot film measurements	57

NOMENCLATURE

A	Vortex generator constant in equations (2.17) and (2.18)
a	Vortex core radius
B	Constant in calibration of hot film anemometer
C	Constant in calibration of hot film anemometer
c_{po}	Reference value for specific heat at constant pressure
D_e	Vortex generator exit diameter
D_p	Piston diameter
d	Vortex ring core diameter
dl	Line element
ds	Elemental area
d_s	Characteristic diameter of probe stem
E	Voltage output of hot film anemometer
E_a	Voltage output of hot film anemometer at ambient measurement temperature
E_{cor}	Voltage output of hot film anemometer corrected for temperature
$G_1, G_2, .. G_n$	Measured independent variable
$\Delta G_1, ..$	Uncertainty in measured independent variable
k_1	Hot film probe yaw factor
k_2	Hot film probe pitch factor
L	Characteristic length (probe stem diameter)
L_p	Piston stroke length
M_1	Mach number inside the cylinder cavity
n	Constant in calibration of hot film anemometer
O.H.R.	Hot film probe overheat ratio

P	Piston velocity correction factor
Q	Value calculated from experimental measurements
ΔQ	Uncertainty in value calculated from experimental measurements
R	Vortex ring radius
R_g	Gas constant
r	Radial distance
r_o	Radius of exit of vortex generator
Re_M	Reynolds number at exit of vortex generator
Re_1	Reynolds number inside the cylinder cavity
St	Strouhal number
T_a	Ambient measurement temperature
T_{cal}	Temperature at which calibration of hot film anemometer was conducted
T_o	Duration of piston stroke
T_s	Mean temperature of hot film probe
T_1	Temperature of fluid inside the cylinder cavity
T_2	Temperature of fluid outside of the cylinder
t	Time
t_c	Time required for core to pass over hot film probe
$\overline{U}$	Mean flow velocity in x direction
$\overline{U}_e$	Average velocity at exit of vortex generator
U_{eff}	Effective cooling velocity of the hot film probe
$\overline{U}_{eff}$	Mean effective cooling velocity of the hot film probe
U_{max}	Velocity at inner edge of vortex core
$U(O)$	Flow velocity

U_o	Centreline velocity at exit of vortex generator
U_p	Piston velocity
U_{pmax}	Maximum piston velocity
$\overline{U}_p$	Average piston velocity
U_{rot}	Rotational velocity along core circumference
U_T	Vortex ring translational velocity
U_x	Flow velocity in the x direction
U_y	Flow velocity in the y direction
U_z	Flow velocity in the z direction
U_∞	Tunnel cross flow velocity
u	Velocity
$\overline{V}$	Velocity
$\overline{W}$	Mean flow velocity in the z direction
x	Distance in direction perpendicular to the plane of the vortex generator exit
α	Angle of orientation of probe in x-y plane
β	Vortex ring tilt angle
ψ	Hot film probe yaw angle
Γ	Circulation
Γ_c	Core circulation
Γ_m	Measured vortex ring circulation
Γ_o	Initial circulation of vortex ring
Γ_T	Total ring circulation
γ	Ratio of specific heats
μ_1	Viscosity of fluid inside the cylinder cavity

ρ_1	Density of fluid inside the cylinder cavity
θ	Hot film probe pitch angle
ν	Kinematic viscosity
ω	Fluctuation frequency

CHAPTER I
INTRODUCTION

The mixing of a fluid injected into a cross flow is a physical phenomenon which has many important engineering applications. One of the major issues in the development of supersonic combustion is the need to improve the efficiency of the mixing of fuel and air. Additionally, today's heightened environmental awareness has lead to an increased interest in the problems associated with the mixing of industrial plant discharges with the surrounding environment.

Vakili (1 and 2) has shown that a pulsed jet can have superior mixing characteristics compared to a steady jet. Low frequency pulsation results in the formation of vortex rings which are able to offer enhanced mixing because of two inherent properties, they penetrate further into a cross flow because of their self induced velocity and they have an increased entrainment rate because of their concentrated vorticity. In light of these properties the kinematics of vortex rings are of great interest.

The method of generating a vortex ring plays an important part in determining the kinematics of the ring. As discussed by Vakili (1) and Didden (3), when a vortex ring is generated by the impulsive motion of a piston the characteristic parameters of the fully developed ring depend on the piston stroke length, the piston velocity profile, the cylinder exit geometry, and the ratio of cross flow velocity to ring translational velocity. While much is known about the effects of exit geometry and the effects of the ratio of cross flow to translational velocity, the influence of the piston stroke length on ring motion, in a cross flow, is not as well understood.

This thesis focuses on the effects that the variation of piston stroke length have on the kinematics of impulsively generated vortex rings. Four chapters follow this introduction. The next chapter is a review of the vortex ring theory that is relevant to the subject research. Chapter III explains the experimental setup and chapter IV reports on the analysis of the experimental results. Finally, conclusions and recommendations are presented.

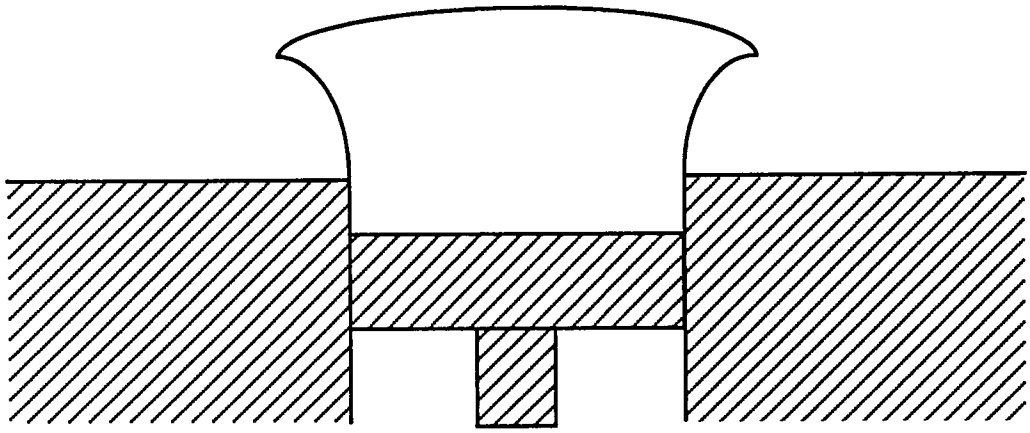
CHAPTER II
TECHNICAL REVIEW

Since the formation of a vortex ring is a phenomenon involving shear forces, a complete description of a vortex ring requires the use of a viscous fluid model. A vortex can be formed by the application of an impulsive force to a fluid in the presence of a sharp boundary. An example of this effect is the vortex ring formed by a piston forcing fluid into a surrounding fluid. Essentially, the ring forms when vorticity, which is present in the boundary layer adjacent to the cylinder wall, causes the flow to curl up as the fluid in the cylinder is ejected into the surrounding stream.

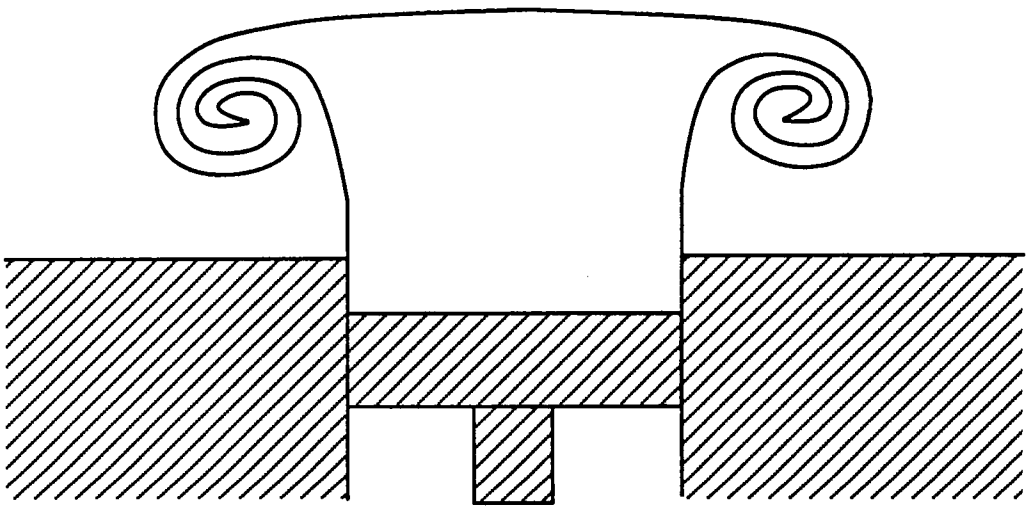
When the fluid is set into motion by the piston, viscous shear creates a velocity gradient at the cylinder walls. Batchelor (4) stated that the requirement for no slip at a solid boundary demands infinite vorticity at the solid wall. Thus the cylinder wall is a source of vorticity. This vorticity diffuses into the cylindrical slug of fluid as the slug moves under the drive of the piston. The result of this diffusion is the growth, out from the cylinder wall, of a boundary layer of vorticity.

The classic explanation of the formation of a piston generated vortex ring proposes that when the fluid passes over the sharp edge of the cylinder exit a surface of discontinuity or vortex sheet is formed. This vortex sheet then rolls up to form a vortex ring. Magarvey and MacLatchey (5) pointed out that this model fails to adequately explain how fluid mass is incorporated into the ring and presented qualitative experimental results that illustrate how the original cylindrical slug of fluid rolls about a circular axis to form a ring.

Their photographs of a cylindrical slug of smoke mixed with air showed that as the slug moved into the ambient fluid under the force of the piston, its leading edge was flattened and a radial flow out from the cylinder was established. As shown in Figure 2.1, these radial arms then curled inward and entrained fluid from the surrounding ambient. This inward curl of the radial arms is a consequence of the cylindrical slug's vorticity. Magarvey and MacLatchey reported that the spiralling eventually lead to the formation of a fully developed ring with approximately half of the fluid mass in



(a) Initial flattening



(b) Roll up

Figure 2.1. Roll up of vortex ring.

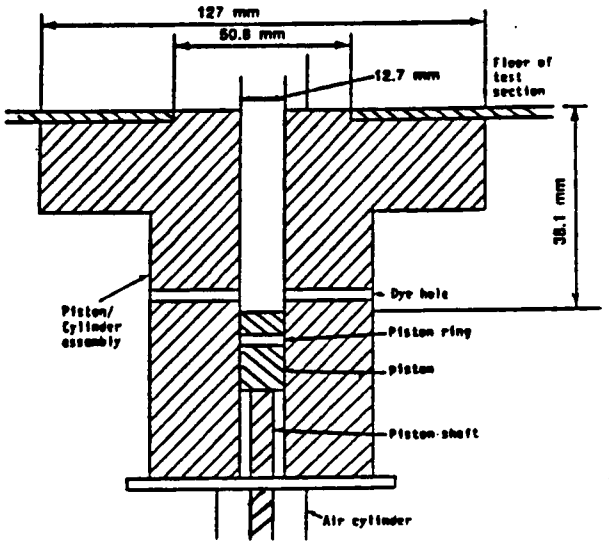
the ring coming from entrained fluid. A common observation amongst researchers is that the process of the cylinder rolling up into a ring is completed by the time the fluid has travelled three cylinder diameters form the orifice.

A literature review reveals that thorough investigation has been conducted on the formation and evolution of vortex rings in quiescent fluid. Invariably, papers such as Didden (3), Maxworthy (6,7, and 8), and Glezer (9) included discussion on the importance of piston stroke length, piston velocity profile, and cylinder exit geometry. Lately researchers have begun to turn their attention to the physics of vortex rings in cross flows. Chang (10) reported on the effects of exit geometry, exit velocity, and cross flow to ring translational velocity ratio; however, the requirement to investigate the effects of piston stroke length variation for rings in cross flow is extant.

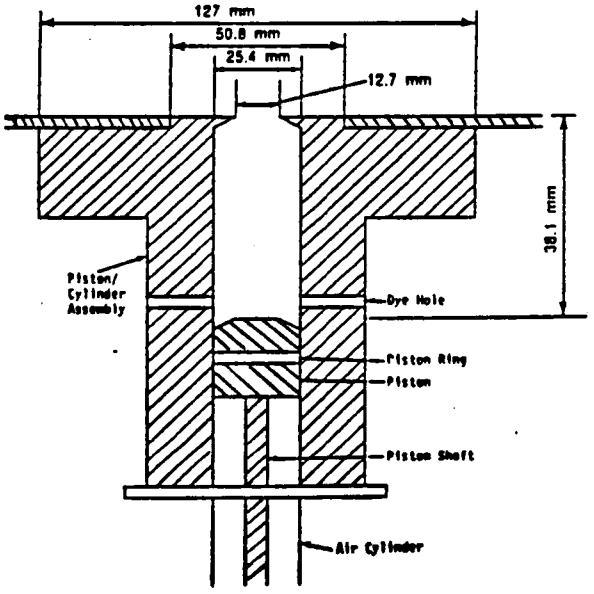
Initial Vortex Ring Characteristics

Given the requirement, this thesis investigates the variation of piston stroke length. The four characteristic parameters of a fully developed vortex ring are circulation, ring diameter, ring core diameter, and translational velocity. In turn, these parameters initially depend on the piston stroke, the piston velocity profile, and the cylinder exit geometry. Chang's (10) experimental results indicated that the cross flow velocity does not have a significant effect on the formation of a vortex ring.

Before discussing the relationship between the three genesis parameters and vortex ring characteristics, a brief outline of the experimental set up is needed. In keeping with earlier research conducted at University of Tennessee Space Institute (UTSI), vortex rings were created using a piston driven generator attached to the floor of the institute's water tunnel. Two different cylinder exit geometries were used for the tests. The straight tube and sharp edged orifice are both shown in Figure 2.2. As for the other two determining parameters, variations in the piston velocity profiles were minimized and the ratio of cross flow velocity to ring translational velocity was varied.



(a) Straight tube configuration



(b) Sharp edged configuration

Figure 2.2. Piston-cylinder configurations.

Circulation

While the models relating ring parameters to the physics of the generator are not complete, it is instructive to look at a simplified description of the relationship between piston stroke length and circulation. As discussed, the slug of fluid moving through the cylinder will have vorticity concentrated in the boundary layer along the cylinder walls. As a result of this vorticity the fluid will have an initial circulation which can be shown to depend on piston stroke length and piston velocity profile.

Glezer (9) used a simple slug model to estimate the flux of vorticity across the plane of the orifice

$$\Gamma = \oint_S (\nabla \times \bar{V}) \cdot d\bar{s} \tag{2.1}$$

$$\frac{d\Gamma_o}{dt} = -\int_0^{r_o} \frac{\partial u}{\partial r} u \, dr \tag{2.2}$$

$$\frac{d\Gamma_o}{dt} = \frac{U_o^2}{2} . \tag{2.3}$$

Integrating with respect to time shows the initial ring circulation's dependence on the piston velocity profile

$$\Gamma_o = \int_0^{T_o} \frac{U_o^2(t)}{2} dt \tag{2.4}$$

$$\Gamma_o = \frac{\overline{U_o^2}\, T_o}{2} . \tag{2.5}$$

By definition, the theoretical calculation of circulation requires an instantaneous velocity. Unfortunately, ascertaining the instantaneous velocity is not practical, thus a mean velocity is used. Assuming a simple straight tube exit geometry with a uniform velocity profile over the piston face and introducing the piston stroke length

$$L_p = \int_0^{T_o} U_o(t)\, dt, \tag{2.6}$$

the mean velocity is expressed as

$$\overline{U_p} = \frac{L_p}{T_o}. \tag{2.7}$$

Introducing equation (2.7) into equation (2.5) yields an expression for initial ring circulation in terms of the piston stroke length

$$\Gamma_o = \frac{L_p^2}{2T_o}. \tag{2.8}$$

Didden (3) and Maxworthy (8) reported results that show that this simple model corresponds approximately with experimental measurement. In particular, Didden (3) showed that with the other three generating parameters fixed, increasing the stroke length results in an increase in measured ring circulation.

A similar calculation can be used to obtain an estimate of the initial circulation for a ring generated with the sharp edged orifice. Continuity requires the mean exit velocity to be

$$\overline{U_e} = \overline{U_p}\left(\frac{D_p}{D_e}\right)^2. \tag{2.9}$$

An approximation of the circulation is then

$$\Gamma_o = \frac{L_p^2}{2T_o}\left(\frac{D_p}{D_e}\right)^4. \tag{2.10}$$

Equation (2.10) illustrates that the exit geometry of the ring generator plays a significant role in determining the initial circulation of the vortex ring.

Interestingly, the relationships given by equations (2.8) and (2.10) are predicted by dimensional analysis. Appendix A contains a generalized dimensional analysis for the functional relationship between initial ring circulation and a comprehensive set of independent parameters.

Experimental results generally reveal that the simple slug model under predicts ring circulation. One reason for this is that the model assumes an average piston velocity when as shown by equation (2.4), the circulation actually depends on the velocity profile. Glezer (9) attempted to account for deviations from the model's average profile by introducing a correction factor

$$P = \int_0^1 \left(\frac{U_p^2}{\overline{U_p}^2}\right) d\left(\frac{t}{T_o}\right) = \frac{\overline{U_p^2}}{\overline{U_p}^2}. \tag{2.11}$$

The Schwarz integral inequality can be used to show that $P \geq 1$ (Appendix B), thus proving that any deviation from a constant velocity profile will produce a greater circulation than that predicted by the slug model. Returning to equation (2.5), equation (2.11) can be used to revise the models for initial ring circulation.

$$\Gamma_o = P\frac{L_p^2}{2T_o} \tag{2.12}$$

and

$$\Gamma_o = P\frac{L_p^2}{2T_o}\left(\frac{D_p}{D_e}\right)^4. \tag{2.13}$$

While this correction factor enhances the model, it does not allow it to accurately predict circulation as the model does not address a number of other factors. Indeed, the velocity profile is still not correctly modelled since the non uniform shape of the profile across the plane of the piston is still not accounted for. In any event, Glezer's analysis demonstrated that when comparing experimental results it is necessary to consider the piston velocity profile.

Didden (3) investigated the formation of vortex rings that were generated by a piston impulsively expelling fluid from a circular nozzle. By taking velocity measurements at regular intervals during the formation of a ring, Didden was able to plot the changes, with time, in the velocity profile at the exit plane. As illustrated in Figure 2.3, he found that in the early stages of the piston's motion a starting flow at the nozzle's edges produces a flow velocity $u > U_p$. Thus initially there is a

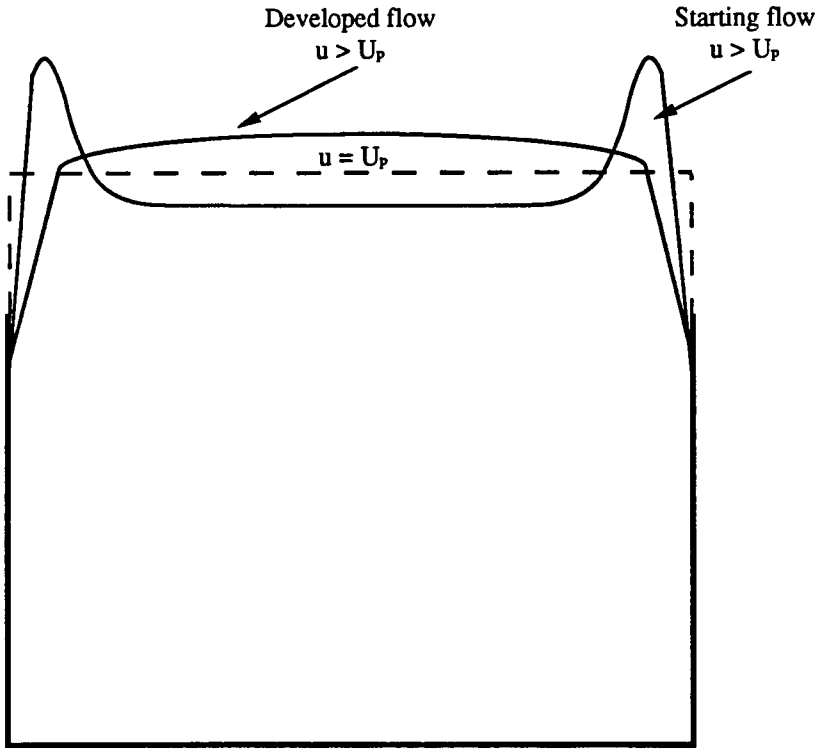


Figure 2.3. Sketch of velocity profiles in exit plane of nozzle used for Didden's (3) experiments.

steep velocity gradient at the nozzle wall and a large vorticity flux into the forming vortex ring. Figure 2.3 also shows that at later times the maximum velocity in the exit plane was found to be greater than U_p. This effect is predictable given the displacement of the boundary layer and the requirement to conserve mass. This also creates an increased velocity gradient at the wall which, like the vorticity flux in the initial stages, is not accounted for by the simple slug model.

The two unmodelled sources of positive vorticity are to some extent countered by another effect associated with the exit geometry of the vortex generator. Didden (3) also made measurements of the velocity field outside of the nozzle which confirmed Maxworthy's (6) prediction that negative secondary vorticity will be produced just outside the orifice. Figure 2.4 shows that the flow induced by the rolling up of the vortex will in turn result in the creation of vorticity of opposite sign which is convected into the forming ring. This source of negative vorticity is the reason that the slug model does not grossly under estimate the initial circulation of the vortex ring. Maxworthy (8) reported that the balance between the production of positive and negative vorticity was weakly dependent on Re_M since the slug model became more representative of measured values of ring circulation as Re_M increased.

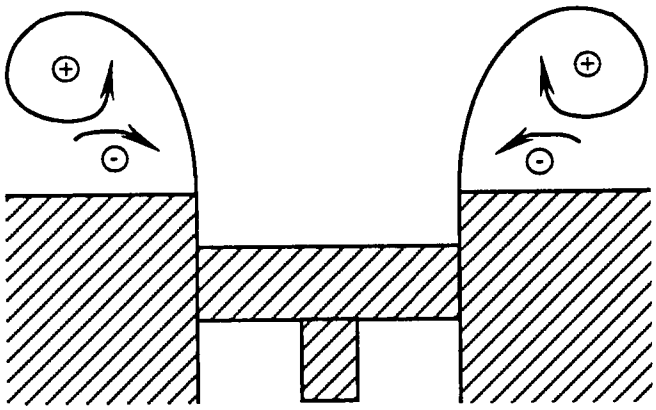
The above paragraph contains the first mention of the parameter Reynolds number in this text. While the reviewed literature does not contain a consistent definition of Reynolds number, a commonly used Reynolds number is based on the characteristics of the vortex generator is

$$Re_M = \frac{\overline{U}_e D_e}{\nu} . \tag{2.14}$$

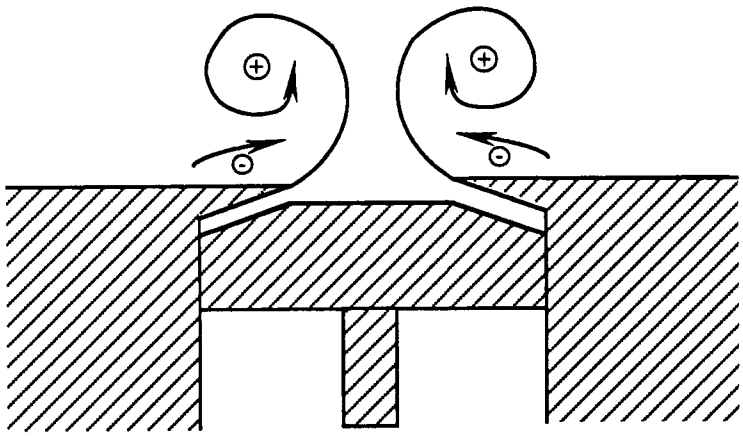
In order to avoid confusion this definition will be used consistently throughout this thesis.

Ring Diameter

As the cylindrical slug of fluid emerges and starts to roll into a ring, the diameter of the ring begins to increase. Didden's (3) measurements for a straight tube nozzle revealed that the ring diameter continued to increase until a maximum was reached at the end of the piston stroke. After the



(a) Straight tube configuration



(b) Sharp edge configuration

Figure 2.4. Production of vorticity during roll up.

maximum, the influence of the generator wall caused a slight decrease in ring diameter. Once the vortex ring had passed out of the wall effect the ring diameter began to increase again.

Maxworthy's (8) experimental results showed that the ring diameter was strongly dependent on the piston stroke length and only weakly dependent on piston velocity. Measurements of ring diameter made 2.5 D_e downstream of the nozzle exit clearly showed that ring diameter increased with increasing stroke length. On the other hand, ring diameter did not vary significantly with piston velocity (Re_M) during experiments conducted throughout the range $Re_M = 1000$ to 7.0×10^4.

The exit geometry of the vortex generator also plays a large role in determining the ring diameter. Chang (10) reported on results obtained with the straight tube and sharp edged exit geometries that were used for the investigation that is the subject of this thesis. He found that, for the same piston stroke length, the initial ring diameter produced by the straight tube was slightly larger than that produced by the sharp edged orifice. Theoretically the initial diameter of the sharp edged orifice ring should be smaller since the geometry produces an inward radial velocity component. However, with the original experimental set up it was not possible to match the piston velocity profiles used with the two configurations, thus Chang's (10) tests did not account for variations in the profiles. For this reason it would be instructive to use similar piston profiles and re-examine the ring diameters produced by the two configurations.

The effect that exit geometry has on vortex ring diameter also has considerable influence on the entrainment properties of the ring. Chang (10) noted that vortex rings formed using the sharp edged exit geometry entrained less fluid than rings formed using the straight tube geometry. One reason for this is the inward radial velocity component produced by the sharp edge. Another is that because the rings generated with the sharp edge have a smaller diameter they also have a smaller surface area through which fluid is entrained.

Core Diameter

Consideration of the effects of the vortex generator on the ring core diameter appear to be limited to the influence of piston stroke length and piston velocity. Maxworthy (8) found that the ring core diameter was weakly dependent on stroke length; core diameter increased slightly with increasing stroke. However, it was found that the core diameter varied with piston velocity, results indicated that

$$d \approx Re_M^{-0.25}. \tag{2.15}$$

Translational Velocity

The relationship between the vortex generator and ring translational velocity is partially explained by the requirement for conservation of mass. As expected, researchers have found that translational velocity increases with increasing piston velocity. In addition, with respect to the two exit geometries used in this study, continuity demands that for the same piston velocity the fluid ejected from the sharp edged orifice will have a larger velocity than the fluid ejected from the straight tube.

However the translational velocity of a vortex ring is not simply a question of conservation of mass. Most of the models describing the self induced translational velocity of a vortex ring give indications of how the generator characteristics effect this parameter. Lamb (11) gave the classic inviscid vortex ring model (assuming $R << a$ and a uniform distribution of vorticity across the vortex core)

$$U_T = \frac{\Gamma}{4\pi R}\left\{\ln\left(\frac{8R}{a}\right) - \frac{1}{4}\right\}. \tag{2.16}$$

Since translational velocity increases with ring circulation, equation (2.8) indicates that for the same piston velocity and exit geometry, increasing piston stroke length should result in an increase in translational velocity. Also any variation in piston velocity profile that results in an increase in ring circulation will produce an increase in velocity.

Another influence of exit geometry is shown by the ring velocity's dependence on ring diameter. Recall that, for the same exit diameter, the inward radial velocity component generated by the sharp edged orifice results in a smaller ring diameter compared to the straight tube exit. Thus even for matching exit velocities the sharp edged orifice would tend to generate a higher translational velocity.

Vortex Ring Kinematics

In the 1970's Maxworthy (6,7, and 8) conducted extensive experiments on the motion of vortex rings. The resulting observations provided a very good description of the physics of a vortex ring translating in an ambient fluid. Two models stemmed from the experiments; the picture for the laminar case being slightly different from that for the turbulent case. As with Reynolds number, the literature presents inconsistent criterion for the classification of laminar versus turbulent vortex rings. However, in this paper, the various ranges will be consistently defined based on the observations of this investigation:

Table 2.1. Classification of flow regimes.

Reynolds Number	Flow Regime
$Re_M < 8000$	Laminar
$8000 \leq Re_M \leq 1.5 \times 10^4$	Transition
$Re_M > 1.5 \times 10^4$	Turbulent

While this research dealt primarily with turbulent vortex rings (Re_M = 8,000 to 7.0 X 10^4), both models will be discussed.

Laminar Vortex Ring

Maxworthy's (6) qualitative description of a laminar vortex ring evolved from a series of flow visualization experiments. Later other researchers, using hot wire anemometer measurements, confirmed the features of this model. Maxworthy (6) noted that a laminar vortex ring consists of a core of concentrated vorticity surrounded by an outer region of weaker vorticity. Vakili's et al (1) measurements indicated that within the core the velocity is highly rotational, varying linearly with distance from the centre of the core. Approximately half of the ring's vorticity is contained within the core. As a ring translates vorticity from its core diffuses into the outer region of weaker vorticity. Another feature of a vortex ring is that as it is translating it is also growing. A ring's growth is due to entrainment. At the edge of the ring vorticity is diffusing from the outer region into the surrounding ambient. Thus as the ring passes through the ambient, the fluid adjacent to its surface becomes entrained into the rear of the ring. In the entrainment process this ambient fluid curls around the original structure forcing the diameter of the ring to increase. In a similar manner the core also increases in diameter as it entrains fluid from the outer region of the ring. Sallet and Widmayer's (12) measurements verified these observations. They found that both ring diameter and core diameter increased linearly with the distance that the vortex traveled. A common observation of researchers has been that while a laminar vortex ring grows as it moves, characteristically, it retains its overall shape. Maxworthy (6) made measurements that showed that the ratio of the ring diameter to the axial length of the ring was approximately constant as a laminar ring translated.

Since the diffusion of vorticity from the ring to the ambient is not discontinuous, there is ambient fluid further away from the surface which has not gained enough vorticity to be incorporated into the ring. This fluid is shed from the ring surface into a wake which trails the translating vortex. Another characteristic of a laminar vortex ring is that its wake tends to be small. This is readily observed when dye is injected into the cylinder of the vortex ring generator prior to firing the piston; the dye highlights the ring-wake structure and shows that a laminar ring's wake is a very thin tail which is often hard to detect. Although diffusion to the ambient is not the only mechanism by which

the translating ring loses vorticity, this thin wake is indicative of the slow rate with which a laminar vortex ring's vorticity dissipates. The other way a vortex ring loses vorticity is by diffusion inside the ring itself since vorticity on opposite sides of the ring's axis of symmetry is of opposite sign.

Keeping in mind that a vortex ring increases in diameter and loses vorticity as it translates, equation (2.16) indicates that its translational velocity will decrease as it moves. Sallet and Widmayer (12) found that their experimental data for laminar vortex rings was described by

$$U_T \approx Ax^{-0.1} \tag{2.17}$$

where A is a constant that depends on the characteristics of the vortex generator and x is the distance the ring has travelled. Their results also confirmed that a laminar vortex ring's vorticity and translational velocity decay very slowly.

Transition

A laminar vortex ring will remain stable and well defined as it propagates. On the other hand, a vortex ring with a Reynolds number in the intermediate range tends to start out as laminar and then undergo transition to turbulence as it translates. The most obvious indicator of transition is the marked change in the ring's wake. Flow visualization experiments have shown that during transition progressively larger quantities of dye (hence vorticity) are deposited into the wake. In this process the wake transforms from a thin tail which is characteristic of a laminar ring to a blooming stream which is characteristic of a turbulent ring.

Many researchers have also documented a more subtle indicator of transition. Maxworthy (8) observed that the onset of transition is characterized by the appearance of a stationary wave which is aligned along the axis of the ring's core (Figure 2.5). As the amplitude of the wave increaseed it tended to break at different locations along the core. While it can be said that turbulence generally follows this breaking process, Glezer (9) in his 1988 paper pointed out that "the details of the vortex ring transition remain unknown." It should be noted that the appearance of the stationary wave does not

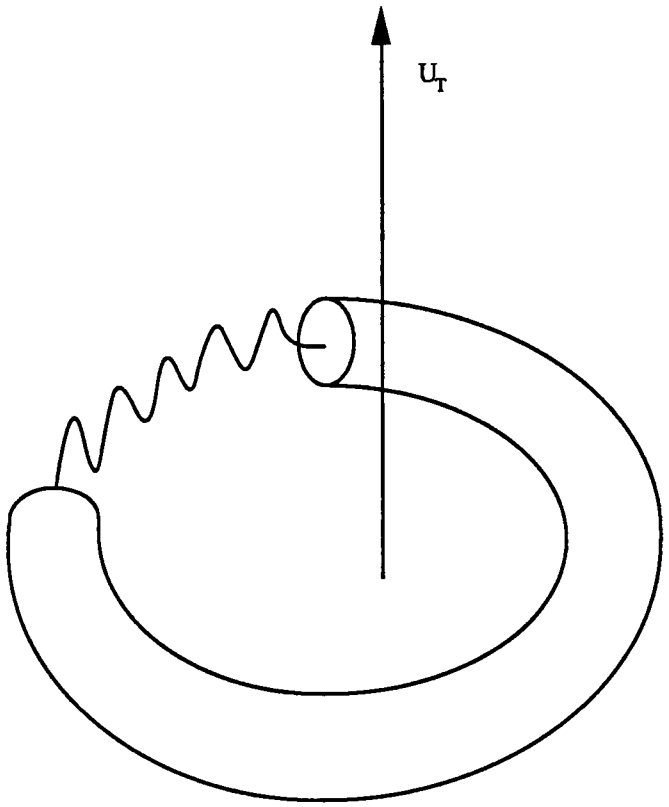


Figure 2.5. Stationary wave core instability during transition.

guarantee transition to turbulence. Glezer (9) found that if the wavelength of the core instability was larger than the generator's stroke length, the amplitude of the waves did not increase enough to result in breaking and transition did not occur.

Maxworthy's (8) results generally indicated that as Re_M increased the appearance of the stationary wave and subsequent break down to turbulence occurred sooner. For Reynolds numbers in the high range, Glezer (9) hypothesized that the core instability is present during roll up and that the breakdown to turbulence is complete by the time the vortex ring is fully developed.

Turbulent Vortex Ring

Maxworthy (7 and 8) presented both qualitative and quantitative results to support a model of turbulent vortex rings. Experiments carried out by a variety of researchers verify that Maxworthy's model is a realistic description of a turbulent vortex ring. As with the laminar case, a turbulent vortex has a core containing roughly half of the ring's vorticity and an outer region of weaker vorticity. However, Maxworthy's (7 and 8) flow visualization results and measurements showed that the core of a turbulent ring is a region with fine scale turbulence and with rotational velocities which are higher than those that might be found in a laminar core. Another difference is that the greater rotational velocities in the core result in a much more abrupt change in the velocity profile at the interface between the core and outer region. This means that there is a greater vorticity gradient between the core and the outer region in the turbulent ring. As with the laminar ring, vorticity will diffuse toward the outer region. Maxworthy (7) noted that the scale of turbulence within the outer region is much larger than the scale within the core.

Like a laminar vortex ring, a turbulent ring entrains fluid and grows as it translates, but, Maxworthy (8) presented data from his own experiments and those of Sallet and Widmayer (12) to show that a turbulent ring grows at a slower rate than a laminar ring. It is suggested that the high rotational velocities within the core limit turbulent fluctuations perpendicular to the core's axis, thus the interface between the core and the outer region is smooth when compared to the laminar interface.

As a result the turbulent ring entrains fluid from the outer region (and hence grows) at a slower rate than its laminar counterpart. Another apparent limitation on the core's growth is that the relatively large scale turbulent flow in the outer region occasionally entrains fluid from the core. At the same time, this large scale turbulence in the outer region results in a rough interface between the ring and the ambient which in turn means that the ring's outer region entrains a large amount of fluid from its surroundings. However, because the core grows very slowly the bulk of this entrained fluid is cast off into the ring's wake and the ring itself grows quite slowly. Sallet and Widmayer (12) presented results showing a slow linear increase in core diameter with the distance that the ring travels and Maxworthy (8) found low linear growth rates for the overall ring diameter.

Since a turbulent vortex ring deposits large quantities of fluid into its wake it is also giving up a significant amount of vorticity as it translates. Both Maxworthy (8) and Sallet and Widmayer (12) made measurements that indicated that a turbulent vortex ring loses a considerable amount of vorticity, relative to a laminar ring, as it moves. Similarly Sallet and Widmayer (12) found that their experimental data for the translational velocity of turbulent vortex rings could be described by

$$U_T \approx \frac{A}{x}, \tag{2.18}$$

a much more rapid decay in velocity when compared to the correlation for their laminar results.

Viscous Vortex Ring Model

Physical descriptions of a translating vortex ring based on flow visualization experiments make it clear that a vortex ring is a viscous phenomenon. Saffman (13) showed that Lamb's inviscid model, equation (2.16), can be extended to account for viscous diffusion giving

$$U_T = \frac{\Gamma}{4\pi R}\left\{\ln\left(\frac{8R}{\sqrt{4\nu t}}\right) - 0.558\right\} \tag{2.19}$$

where $\nu t << R^2$. While this model allows for an increase in core diameter and a decrease in translational velocity, it should be noted that it incorrectly assumes that the ring's vorticity is limited

to the core. When compared with experimental results it tended to over estimate the decay in translational velocity.

Translating Vortex Ring in a Cross Flow

Using flow visualization Chang (10) observed vortex rings in uniform cross flows which tilted as they translated. As shown in Figure 2.6, the forces that result from the differences in relative velocity introduced by the cross flow cause the rear of the vortex ring to tilt up into the flow. Manyresearchers have attempted to describe this phenomenon by representing the vortex ring as a Rankine vortex and then using the Kutta-Joukowski theorem to approximate the forces acting on the ring. Recently, Caruthers (14) has shown that when combined with a uniform cross flow a Rankine vortex does not tilt. Caruthers has also shown that the tilting motion can be modelled by adding a singular vortex sheet with zero net circulation to the surface of the Rankine vortex as this introduces a required discontinuity in tangential velocity at the surface.

Summary

In the above a number of papers on vortex ring kinematics have been reviewed in order to present the relationships between the determining experimental parameters (piston stroke length, piston velocity profile, cylinder exit geometry, and cross flow velocity) and the dependent vortex ring characteristics (ring circulation, ring diameter, ring core diameter, and ring translational velocity). Additionally, it has been noted that, to the author's knowledge, a study of the effects of the variation of the generator's piston stroke length on the characteristic parameters of a vortex ring in cross flow has not been conducted. Thus the subject of this thesis is the relationship between the vortex generator piston stroke length and the characteristic parameters of a vortex ring.

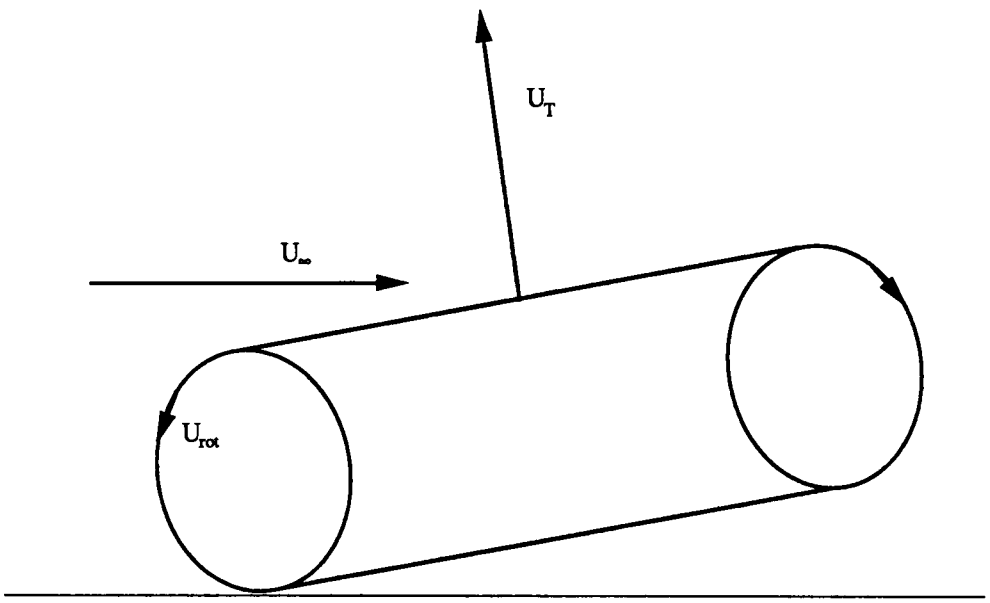


Figure 2.6. Tilting of vortex ring in cross flow.

CHAPTER III
EXPERIMENTAL PROCEDURE

In order to study the relationship between stroke length and the characteristic parameters of a vortex ring, vortex rings were created in UTSI's water tunnel using a piston driven vortex generator. Both flow visualization and hot wire anemometer experiments were carried out. Experiments were conducted with both a quiescent tank and with a cross flow in order to allow for comparison between the two conditions. A thorough description of the water tunnel laboratory (including the water tunnel, the calibration channel, the hot film anemometer system, and many aspects of the vortex generator) was given by Chang (10). A brief description of the facilities, with more detailed explanations of features unique to this research, is included below.

Water Tunnel

The water tunnel is a closed loop with flow driven by a propellor powered by a 1 hp electric motor. Water flow in the tunnel ranges from 0.5 in/sec to 24 in/sec. The test section of the tunnel is shown in Figure 3.1. In the test section, the tunnel walls are made of plexiglass in order to facilitate flow visualization. The test section also contains a false floor which allows the boundary layer to be evaluated. Finally, Figure 3.1 also shows the fitting which permitted the vortex generator to be installed underneath the test section.

Vortex Generator

The vortex generator system, consisted of four main components and is shown in Figure 3.2: a computer program coordinated the operation of the vortex generator, the piston cylinder assembly impulsively ejected a slug of fluid into the test section, the air cylinder served as the actuator, and the linear potentiometer provided a means of recording the piston velocity profiles.

The piston cylinder assembly is as shown in Figure 2.2. As mentioned in Chapter II, tests were conducted using both a straight tube and a sharp edge exit configuration. The aluminum cylinder

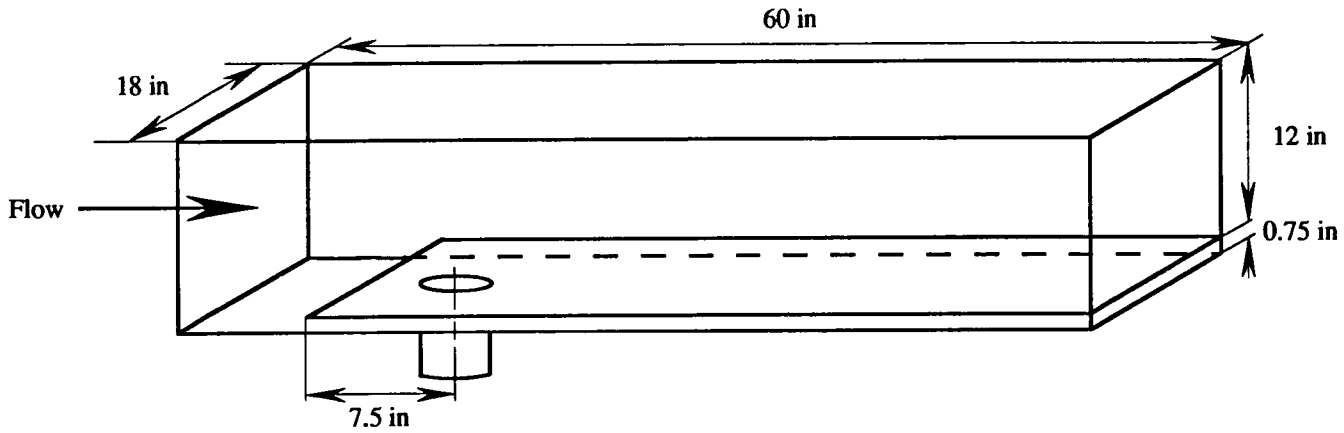


Figure 3.1. Water tunnel test section.

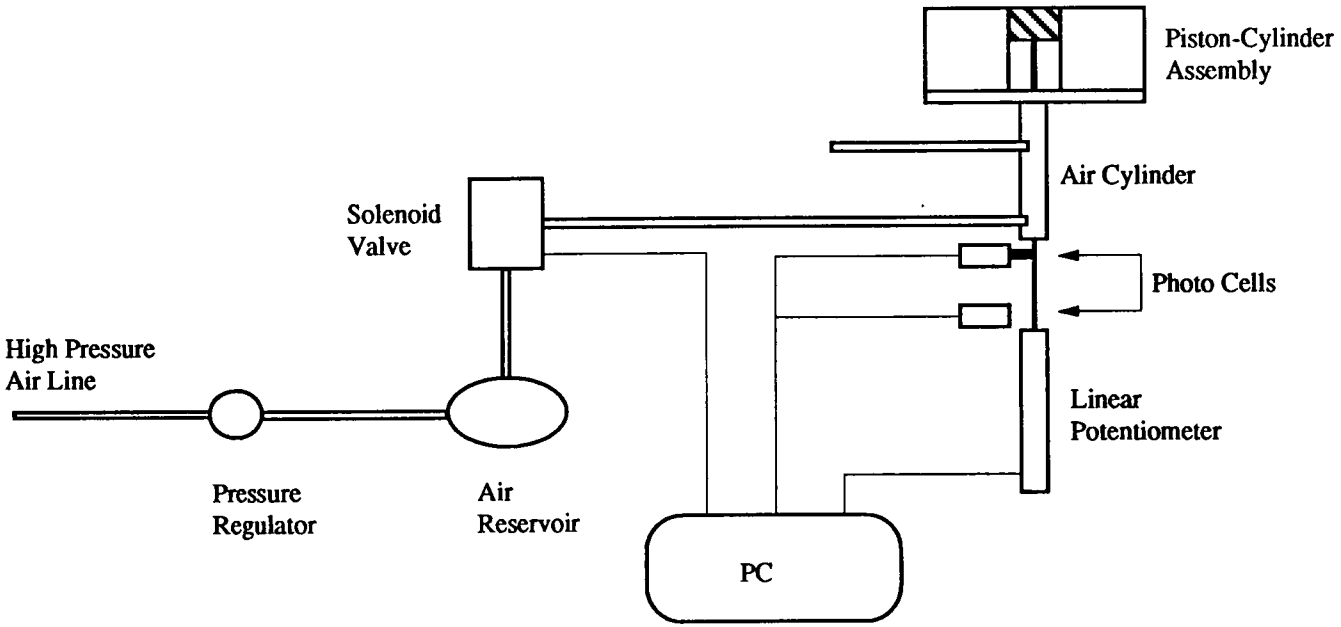


Figure 3.2. Vortex generator system.

was machined to accept the sharp edged piston (Figure (2.2 (b)). An aluminum insert was also used to adapt the cylinder to the smaller diameter of the straight tube piston (Figure (2.2 (a)). Also shown on Figure 2.2, the cylinder and insert were tapped at 90° intervals to provide dye ports for flow visualization. The two pistons were machined from copper and were each fitted with a silicone rubber O-ring.

The actuator for the piston cylinder assembly was a 3/4 inch bore double acting air cylinder (Bimba part number 04-1.0-DXDE). As shown in Figure 3.2, air was regulated from a high pressure line. Airflow to the air cylinder was controlled by a solenoid valve (ASCO model 8342C3) and an air reservoir was installed between the solenoid and the regulator in order to ensure that a uniform pressure was applied to the actuator. Firing of a piston, which was attached to the upper shaft of the air cylinder, was initiated by a signal from the personal computer (PC) which opened the solenoid valve. The velocity of the piston, hence the velocity of the slug of fluid, could be varied by applying different air pressures to the air cylinder. Pressures used in this work ranged from 35 psi to 90 psi.

The 04-1.0-DXDE air cylinder came with a 1.0 inch stoke. A set of aluminum spacers were used to vary the stroke length. Since the lower shaft of the air cylinder was coupled to the shaft of the potentiometer, placing a spacer on top of the potentiometer decreased the stroke by the length of the spacer. The stroke lengths tested for this investigation were 0.8 inches, 0.5 inches and 0.25 inches.

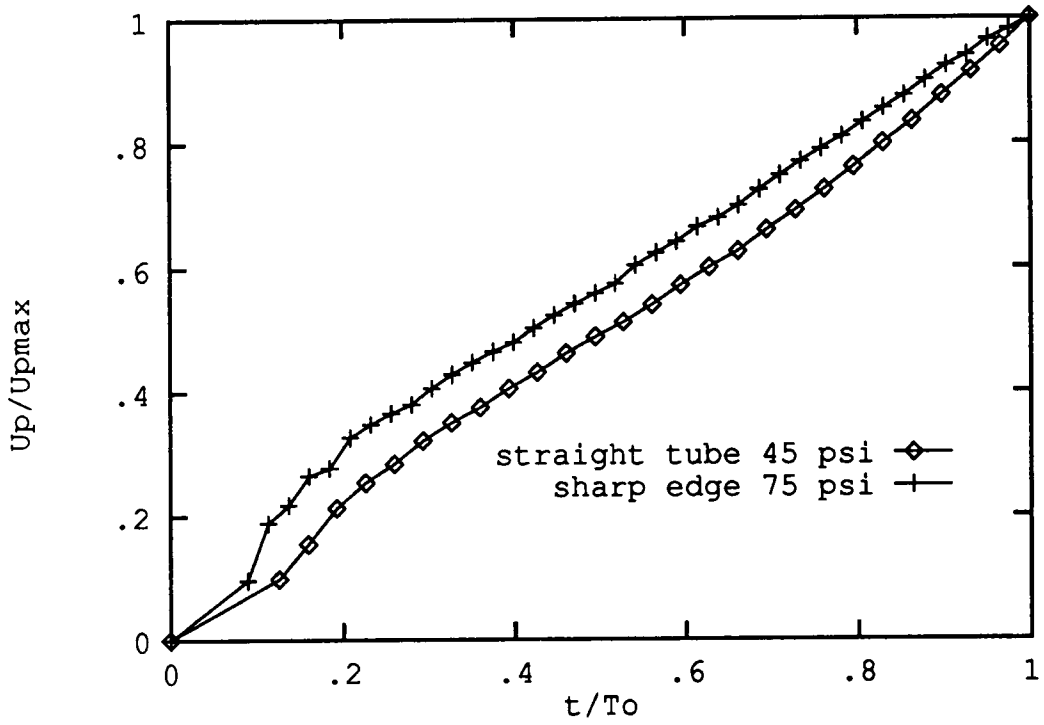
As explained in chapter II, it was necessary to take the piston velocity profile into consideration when evaluating the characteristics of a piston generated vortex ring. In order to record piston velocity profiles, the vortex generator system included a pair of photo-cells and a linear potentiometer. As shown in Figure 3.2, the photo-cells were positioned such that triggering the first photo-cell started the PC's timer and passing through the second photo-cell switched off the timer. Since the air cylinder was connected to the potentiometer it was possible to record the displacement of the piston at regular time intervals during each stroke. The controlling program on the PC included

code which numerically differentiated the piston displacement versus time data in order to obtain a record of piston velocity profiles.

Piston Velocity Profiles

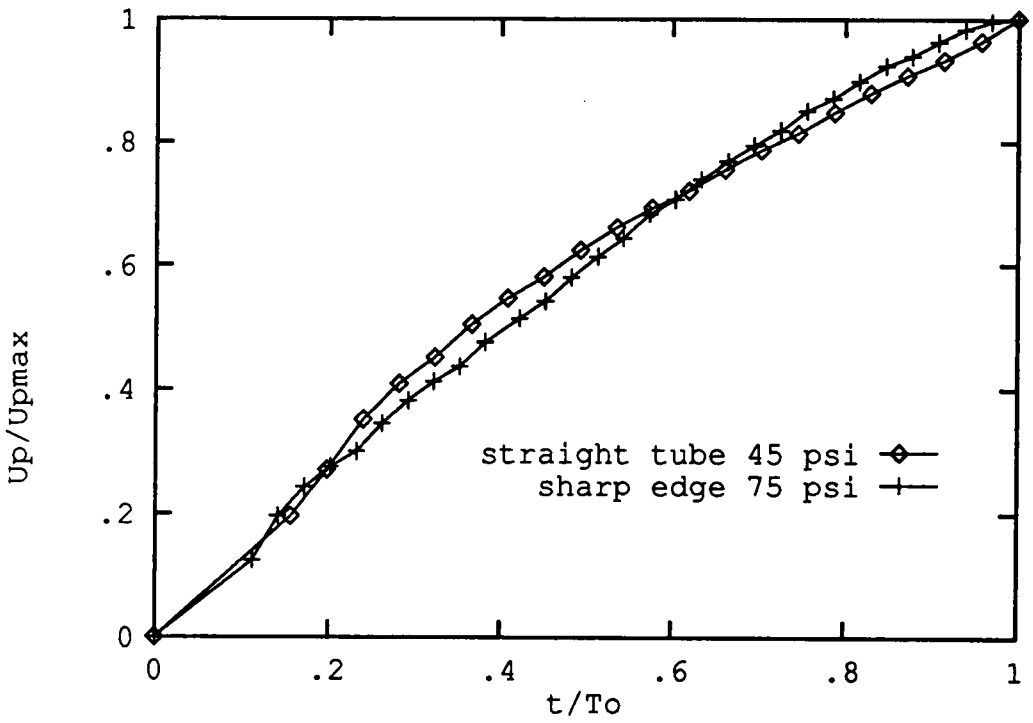
As noted, the characteristics of a piston generated vortex ring depend, in part, on the piston's velocity profile. Thus before proceeding with the experiments to evaluate the characteristic parameters, the first step was to select exit geometry-pressure test configurations with velocity profiles that were similar enough to warrant comparison. For this purpose tests were run at 5 psi intervals between 35 psi and 90 psi to obtain velocity profiles for both configurations.

Initially these tests were run using the experimental set up as it was originally conceived, with a smaller 7/16 inch bore air cylinder actuator and without an air reservoir. At first no suitable match could be obtained between the two pistons because the acceleration of the larger and heavier sharp edged piston was very low during the initial stages of its motion. In an attempt to remedy this problem by reducing pressure losses, a shorter line was used to connect the solenoid valve and the high pressure air supply line. This yielded some improvement, however because the sharp edged piston still suffered from an unacceptable lag in its initial motion an air reservoir was added between the solenoid valve and the high pressure supply line. While this brought the shape of the sharp edged piston's velocity profiles closer to those of the straight tube piston, at this stage it became apparent that a match would not be obtained using the 7/16 inch air cylinder as it could not provide enough force to over come the inertia of the larger piston. The 7/16 inch air cylinder was then replaced with the larger 3/4 inch bore actuator and after this change it was possible to produce similar profiles for the two piston configurations. Figure 3.3 (a-c) contains examples of the types of similar profiles which were selected.



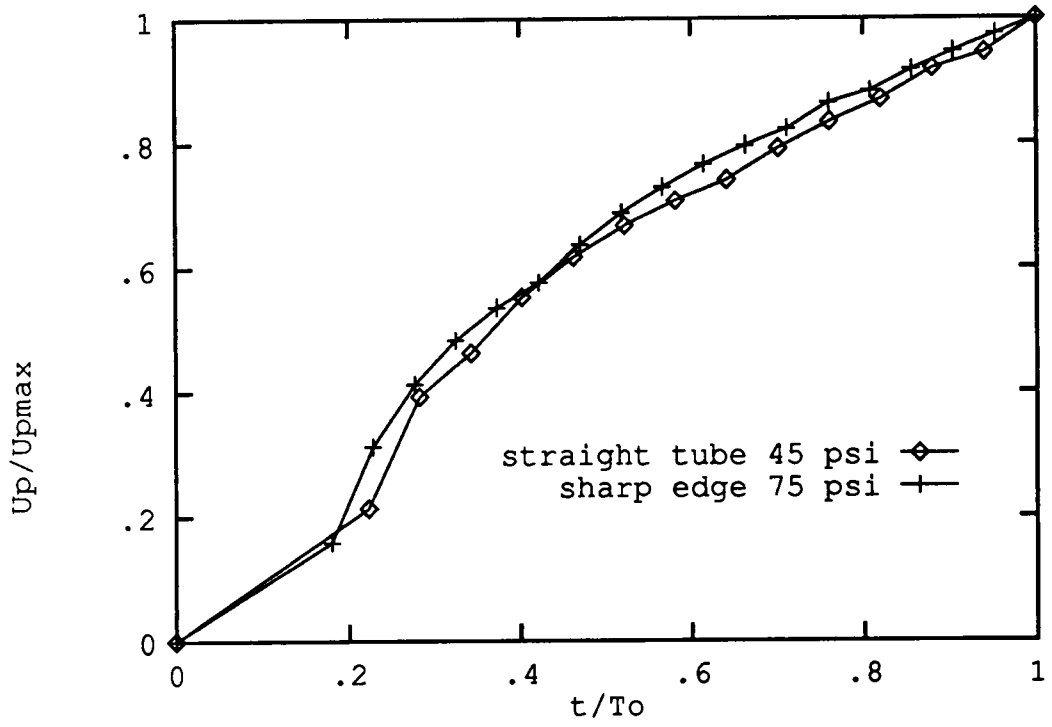
(a) Piston stroke length 0.8 inches

Figure 3.3. Piston velocity profiles of test configurations used for the analysis of circulation.



(b) Piston stroke length 0.5 inches

Figure 3.3. Continued



(c) Piston stroke length 0.25 inches

Figure 3.3. Continued

Hot Film Anemometer Measurements

Hot film anemometry was used to determine the velocity within the translating vortex rings. Mean velocity measurements were obtained using a TSI model 1212-60W hot film probe connected to a TSI model IFA 100 flow analyzer and operated at a constant temperature. Fingerson (15) noted that the effects of free convection from the hot probe could be minimized by using a low overheat ratio (hence probe temperature) where the overheat ratio is defined as

$$O.H.R. = \frac{T_s - T_a}{T_a} . \tag{3.1}$$

Thus the probe was operated at a relatively low overheat ratio of 1.04. Analogue voltage output from the flow analyzer was converted to a digital signal using a Scientific Solution's Lab Master analogue to digital converter and then stored on a PC.

Calibration of Probe

An anemometer can be calibrated by correlating known velocities with the voltage output of the system. Jorgensen (16) gave the correlation between the voltage output and the velocity of the fluid which transfers heat from the probe as

$$E^2 = C + BU^n . \tag{3.2}$$

Where the constants B, C, and n are determined by a least squares curve fit. When taking measurements at temperatures which are different from those for which the voltage-cooling velocity calibration has been obtained, the voltage in equation (3.2) must be corrected for temperature. Fingerson (15) gave the correction as

$$E_{cor} = \left[\frac{T_s - T_{cal}}{T_s - T_a}\right] E_a . \tag{3.3}$$

Calibration was conducted in the calibration channel which is used with UTSI's water tunnel. The channel is a section of plastic pipe which has been turned into a trough by cutting it open as shown in

Figure 3.4. Steel rails are positioned over the trough and an aluminum traverse which carries the probe is mounted on the rails. The traverse is moved by a steel cable which runs through the traverse and over two pulleys fixed at each end of the channel. Drive is provided by a Motomatic E-500 D.C. servo motor. Also shown in Figure 3.4 are the three photo-cells used in the timing of the traverse's motion. The first and second photo-cells demarcate a distance over which the traverse can accelerate to a constant speed and the second and third photo-cells demarcate the distance over which the traverse (hence probe) velocity can be calculated. Probe velocity can then be correlated with the recorded voltage output. For this work calibration was conducted at a temperature of 68° F. The resulting calibration curve is shown in Figure 3.5.

Directional Sensitivity of Probe

For this discussion of the probe's directional sensitivity, Figure 3.6 illustrates the relationship between the velocity components of the flow and the probe orientation. For an infinitely long probe the effective cooling velocity would be simply the component of the fluid velocity normal to the probe

$$U_{eff} = U_x. \tag{3.4}$$

However for the case of a finite length probe, the velocity component parallel to the probe also contributes to the effective cooling velocity. In order to address this contribution Hinze (17) added a term to equation (3.4)

$$U_{eff}^2 = U_x^2 + k_1^2 U_y^2 . \tag{3.5}$$

Here k_1 is known as the yaw factor and is determined empirically. Jorgensen (16) also noted that the probe and its supports interfere with the flow and that this interference varies with the inclination or pitch of the flow. In order to compensate for this effect he introduced a pitch factor such that

$$U_{eff}^2 = U_x^2 + k_1^2 U_y^2 + k_2^2 U_z^2 . \tag{3.6}$$

Here k_2 is the empirically determined pitch factor.

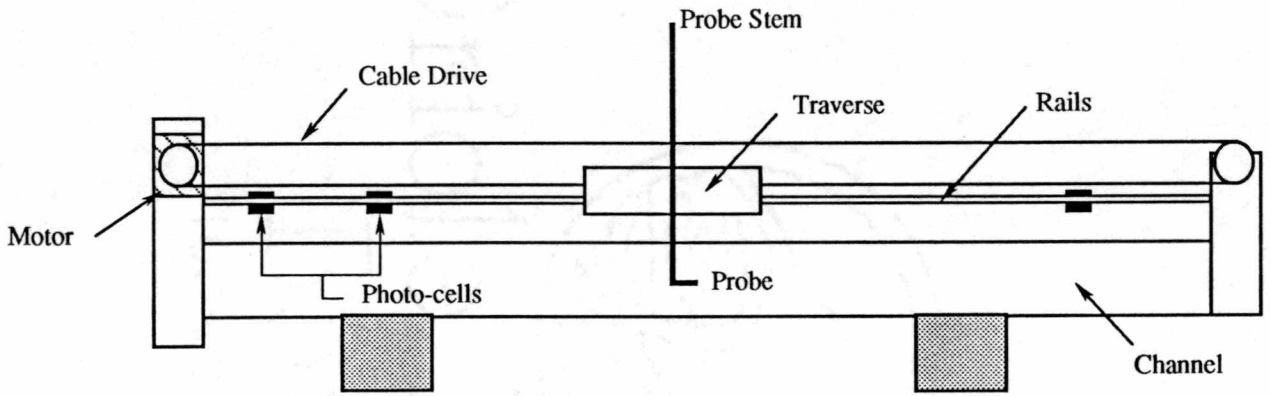


Figure 3.4. Anemometer caibration channel.

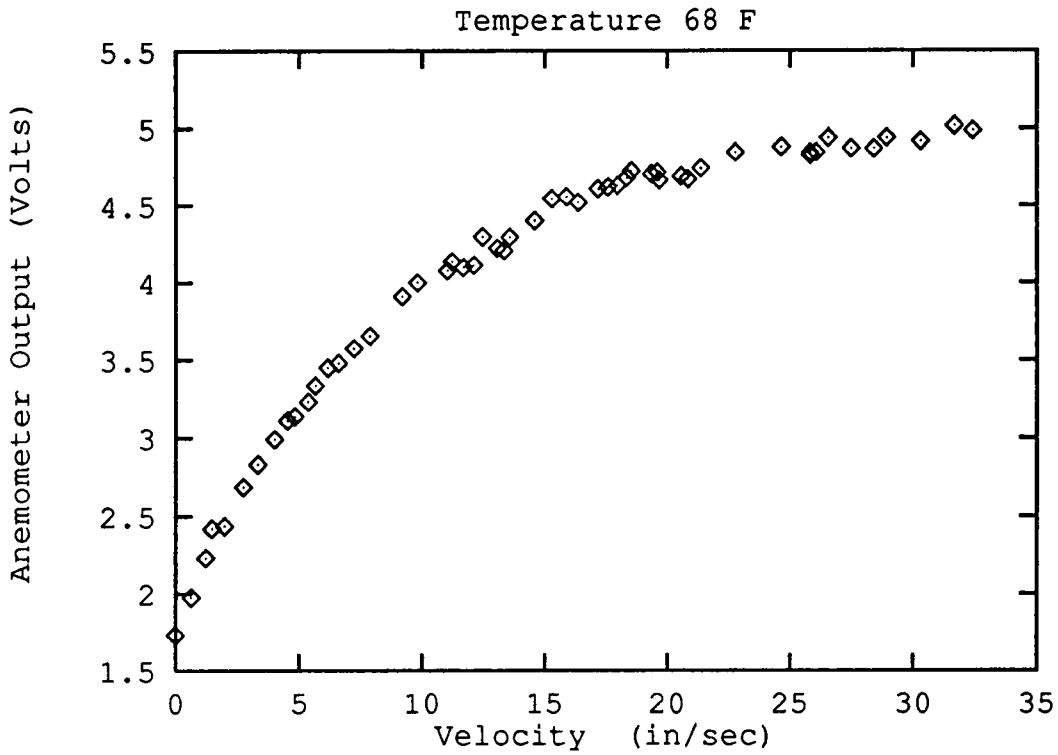


Figure 3.5. Typical calibration curve for hot film probe.

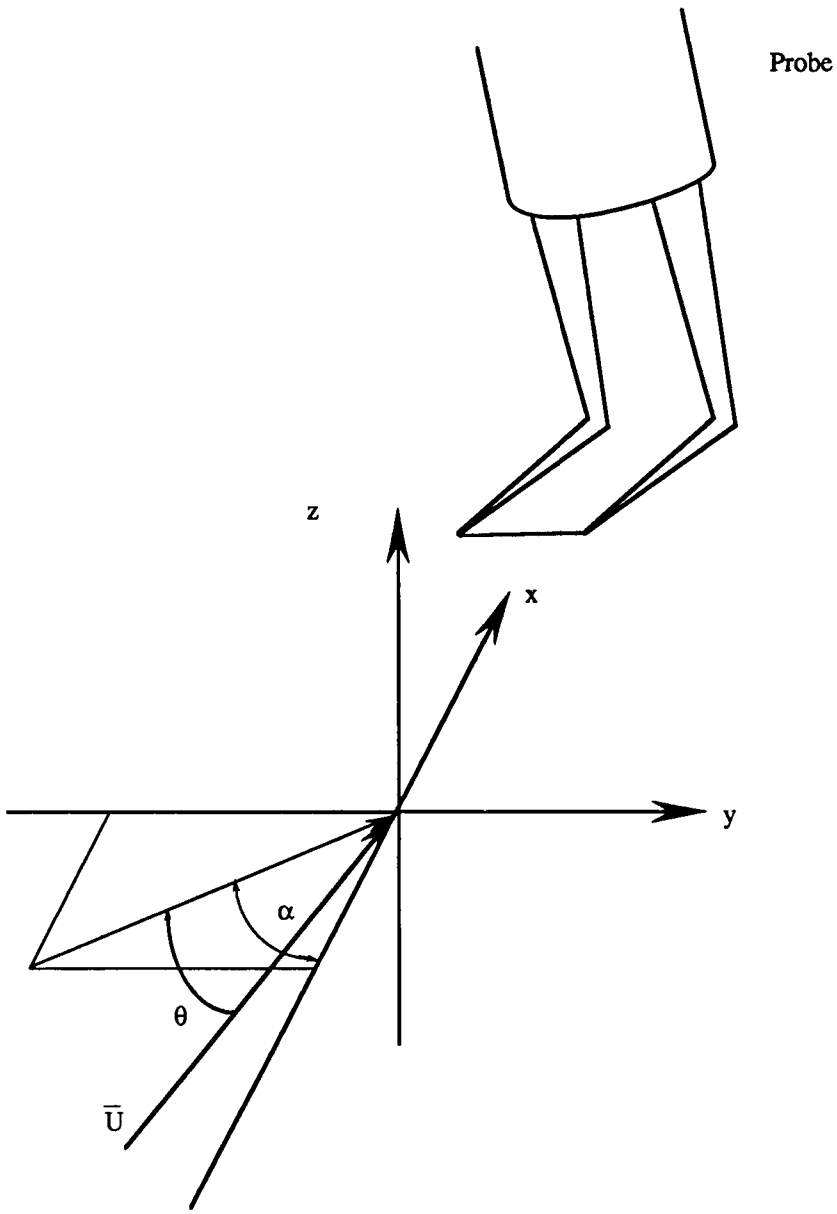


Figure 3.6. Pitch and yaw angles relative to probe.

The yaw and pitch factors vary with yaw and pitch angles respectively. In order to determine these two factors it is noted that for zero pitch angle ($\theta = 0$)

$$U_{eff}^2 = U^2(O)(\cos^2\psi + k_1^2 \sin^2\psi) \tag{3.7}$$

and for zero yaw angle ($\psi = 0$)

$$U_{eff}^2 = U^2(O)(\cos^2\theta + k_2^2 \sin^2\theta)\,. \tag{3.8}$$

Introducing equation (3.2) into equations (3.7) and (3.8) the yaw factor can be expressed as

$$k_1 = \frac{1}{\sin\psi}\left[\left(\frac{E^2(\psi) - C}{E^2(O) - C}\right)^{\frac{2}{n}} - \cos^2\psi\right]^{\frac{1}{2}} \tag{3.9}$$

and the pitch factor as

$$k_2 = \frac{1}{\sin\theta}\left[\left(\frac{E^2(\theta) - C}{E^2(O) - C}\right)^{\frac{2}{n}} - \cos^2\theta\right]^{\frac{1}{2}}\,. \tag{3.10}$$

Jorgensen (16) found that a single yaw factor could be used for all measurements by choosing a value that corresponds to a yaw angle at the upper end of the range of angles used for an experiment. He reported that the error introduced by this expedience was less than 10%. Thus for this experimental work a single yaw factor, evaluated at a yaw angle of 90°, was used. It was also found that the pitch factor varies only slightly with pitch angle. Jorgensen's (16) work indicated that adopting a constant $k_2 = 1.0$ would introduce an error of less than 5%. As a result a value of $k_2 = 1.0$ was used throughout this investigation.

Mean Velocity Components

Chang (10) expressed the significant mean velocity components at a point in the flow as functions of two mean effective cooling velocities at that point: one with the probe oriented perpendicular to the cross flow ($\alpha = 0°$) and the other with the probe oriented parallel to the cross flow ($\alpha = 90°$). The result is

$$\overline{U^2} = \frac{1}{k_2^2 - k_1^2}\left(\overline{U_{eff}^2}(\alpha=90°) - \overline{U_{eff}^2}(\alpha=0°)\right) \tag{3.11}$$

and

$$\overline{W^2} = \frac{1}{k_2^2 - k_1^2}\left(k_2^2\,\overline{U_{eff}^2}(\alpha=0°) - k_1^2\,\overline{U_{eff}^2}(\alpha=90°)\right). \tag{3.12}$$

After the probe was calibrated and the yaw factor determined, equations (3.11) and (3.12) were incorporated into a computer program which was used to reduce the experimental data.

Fluctuation in the Measurement of Cross Flow Velocity

Prior to taking measurements of the velocities of translating vortex rings, measurements of tunnel flow velocities were taken in order to investigate the reliability of the hot film anemometer set up. Several cross flows in the 2.0 in/sec to 6.0 in/sec range proposed for use during the experiments were investigated.

The results of a number of these tests showed an unacceptable level of data scatter. As a result, the tests were repeated with the anemometer output run through an oscilloscope for a frequency spectrum analysis. The spectrum analysis showed that the frequencies of the largest velocity fluctuations were in the range of 1 Hz to 3 Hz. This information suggested that the fluctuations might have been caused by vibrations introduced by the probe stem shedding vortices. An analysis revealed that the Reynolds number for the tests was in the range $175 < Re < 550$, where

$$Re = \frac{U_\infty d_s}{\nu} \tag{3.13}$$

and that the Strouhal number

$$St = \frac{\omega L}{U_\infty} \tag{3.14}$$

for the cases subject to fluctuations was in the neighbourhood of St = 0.2.

A heavy thick thread was then spiralled around the probe stem with the aim of minimizing oscillations caused by vortex shedding. Follow up tests indicated this technique reduced fluctuations in the 1 Hz to 3 Hz range to an acceptable level, thus it was subsequently used when taking measurements in the presence of a cross flow.

Vortex Ring Velocity Measurements

The velocities within a vortex ring are of great interest in that they contain information on all of the characteristic parameters of a ring. Velocity profiles were obtained from a series of measurements taken on a line through the centre of a vortex ring as shown in Figure 3.7. Each series of measurements was taken at a distance of 7 D_e, above the vortex generator. In order to supply a means of accurately moving the probe to different locations, the probe stem was mounted in a traverse that provided both horizontal and vertical travel. Identification of a vortex ring core could only be made from velocity profiles when a very fine increment between measurement points was used. Thus in the region where it was expected that the core would be found the distance between the measurement stations used, as shown in Figure 3.7 corresponded to the traverse's smallest increment (0.005208 in).

Flow Visualization

Injecting food colouring through the dye ports into the cylinder cavity prior to firing the piston allowed an observer to view the flow structure as the cylindrical slug of fluid rolled up into a vortex ring and translated to the top of the test section. A spatial frame of reference was provided by mounting a 1 inch by 1 inch grid, plotted on white mylar, on the back wall of the plexiglass test section. A reference frame for overhead viewing was provided by a similar grid marked on the white

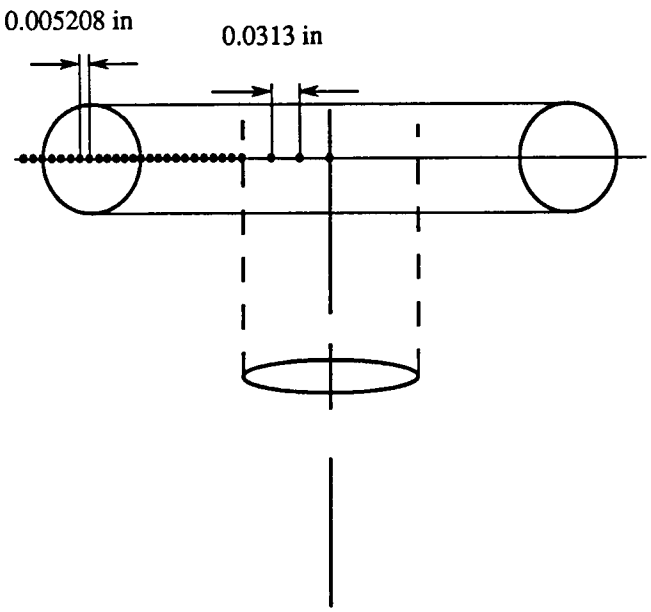


Figure 3.7. Vortex ring velocity measurements.

painted floor of the test section. The high contrast between these white backdrops and the dye also enhanced the visibility of the flow structure. In order to provide a record for analysis, tests were taped using a tripod mounted video camera. The results were then reviewed, at various tape speeds, on a VCR.

Evaluation of Characteristic Parameters

Circulation

Since the analysis required that circulation be quantified, only those test configurations that yielded a reasonable velocity profile correction factor were selected for the analysis of circulation. All of the test configurations which were selected for quantitative analysis are shown in Figure 3.3 (a-c).

For this investigation circulation was evaluated via two approaches. First the initial ring circulation was estimated as per equations (2.12) and (2.13). This method required the evaluation of a velocity profile correction factor. This was done by approximating each of the piston velocity profiles involved (Figure 3.3) as a multi-linear function and the carrying out the integration of equation (2.11).

Then the circulation as a ring translated was estimated from ring velocity measurements using a method described by Sallet and Widmayer (12). They based their estimate of ring circulation on the core circulation. With

$$\Gamma = \oint_L \bar{V} \cdot \bar{dl} \tag{3.15}$$

core circulation is expressed as

$$\Gamma_c = U_{rot}\, \pi d\,. \tag{3.16}$$

Total ring circulation is then related to core circulation by treating the vortex ring as a line vortex. Sallet and Widmayer asserted that this approximation is valid as long as $a << R$. They used the Hamel-Oseen solution for a line vortex where

$$u(r,t) = \frac{\Gamma_T}{2\pi r}\left[1 - \exp(-\frac{r^2}{4\nu t})\right] \tag{3.17}$$

and carrying out the integration of equation (3.15) the core circulation is expressed as

$$\Gamma_c = \Gamma_T\left[1 - \exp(-\frac{r^2}{4\nu t})\right]. \tag{3.18}$$

In order to relate the total ring circulation to the core circulation an expression for the core diameter must be developed. Sallet and Widmayer recommended that equation (3.17) be differentiated with respect to r while t is held constant. Since the maximum velocity within a vortex ring theoretically occurs at the inner edge of the core, the core diameter can be found by setting

$$\frac{\partial u}{\partial r} = 0 \tag{3.20}$$

and solving for r. Evaluating equation (3.20) leads to

$$\exp(-\frac{r^2}{4\nu t})\left[1 + \frac{2r^2}{4\nu t}\right] - 1 = 0 \tag{3.21}$$

which when solved iteratively gives

$$d = 4.483\sqrt{\nu t}\ . \tag{3.22}$$

Equation (3.22) is then substituted back into equation (3.18) which allows one to obtain

$$\Gamma_T = 1.398\Gamma_c\ . \tag{3.23}$$

Ring Diameter

The overall diameter of a vortex ring was determined using flow visualization. With flow visualization the structure of a vortex ring stood out against the test section backdrop, thus ring diameter could be measured on the backdrop's grid.

As the physical mechanism for a vortex ring's growth, entrainment is tied to ring diameter. In order to get a detailed view of the entrainment process during roll up, tests were run with the camera focused on the orifice of the vortex generator. For these experiments a 1/16 inch plastic tube carrying dye was run along the floor of the test section with the end of the tube fixed in place several millimeters upstream of the orifice. Then, just prior to firing the piston, a small amount of dye was allowed to flow to the area around the orifice; however, care was taken to ensure that dye did not flow over and or into the orifice.

Core Diameter

While flow visualization highlights the vortex core to some degree, it does not always clearly delineate between the core and the outer region. Hence a measure of core diameter is best obtained from hot film velocity measurements.

Translational Velocity

Ring translational velocity was evaluated using hot film anemometry. Since the velocity at the centre of a core is the translational velocity of the ring, instantaneous translational velocity was obtained from hot film measurements.

CHAPTER IV
EXPERIMENTAL RESULTS AND ANALYSIS

In the following chapter the experimental results are presented. Specifically, the effects of the variation of piston stroke length on vortex ring characteristics are analyzed. Comparison of the results for the two different exit geometries is also included as well as, for each of these configurations, a discussion of the significance of cross flow.

Circulation

As discussed in chapter III, the measurement of ring circulation requires knowledge of the rotational velocity at the edge of the core and of core diameter. Both of these parameters were obtained from hot film anemometer measurements. Fig 4.1 (a) is a plot of anemometer output versus time for a location through which the centre of a vortex ring core has passed. The two peaks shown in Figure 4.1 (a) are the key to identifying the core of a ring which was moving through a quiescent tank. The peaks were the result of first the top and then the bottom edge of the core passing by the probe. The valley was caused by the centre of the core and thus the voltage at this point is representative of the ring's translational velocity.

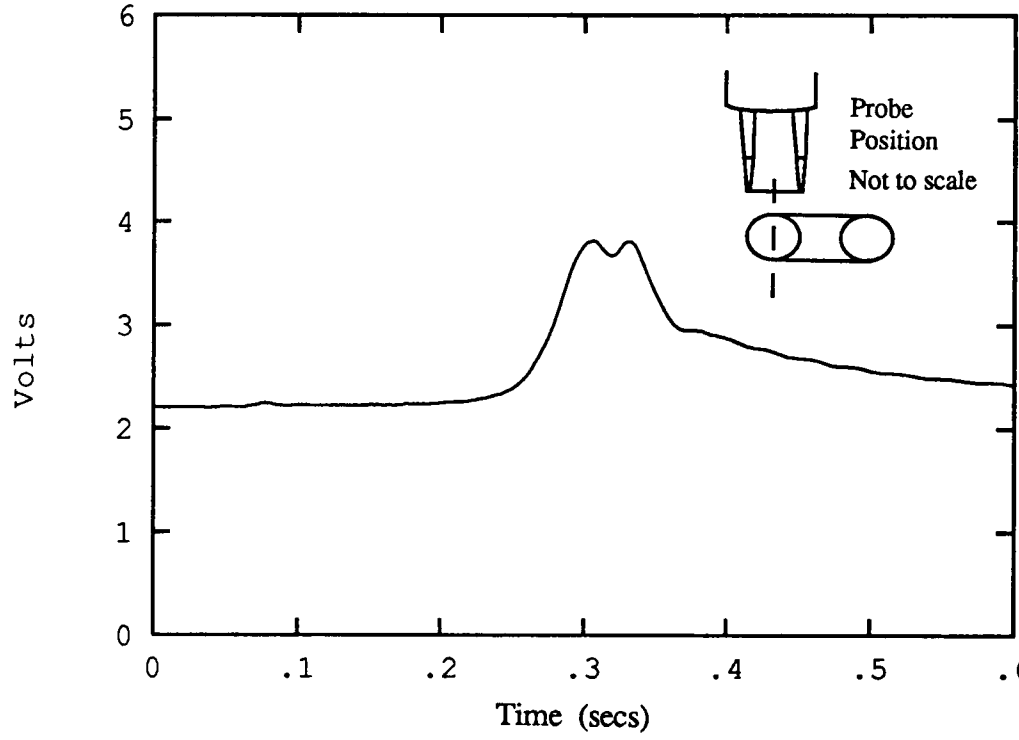
Using the translational velocity and the time difference between the two peaks the core diameter is simply

$$d = U_T t_c . \tag{4.1}$$

At the inner edge of a core, theoretically the velocity will be

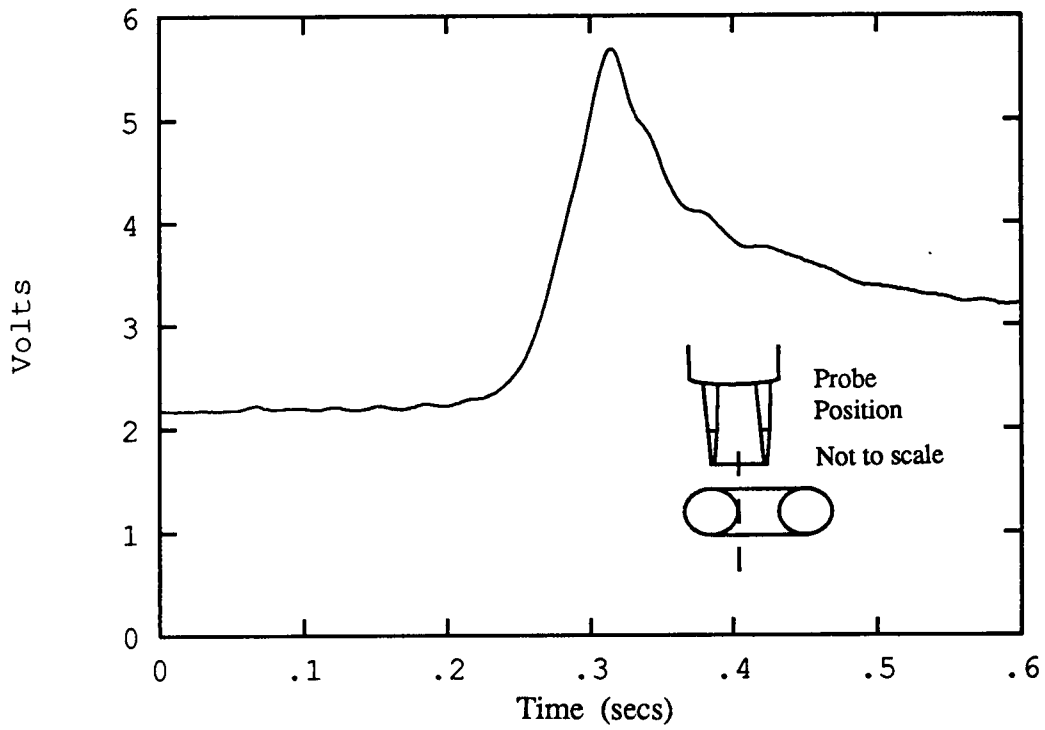
$$U_{max} = U_T + U_{rot} . \tag{4.2}$$

Thus the diameter given by equation (4.1) was used to determine the location of the inner edge of the core and then the velocity at this point and the translational velocity were used in equation (4.2) to



(a) Voltage-time history showing centre of core passing by probe

Figure 4.1. Hot film anemometer voltage-time histories.



(b) Voltage-time history showing inner edge of core passing by probe

Figure 4.1. Continued.

evaluate the rotational velocity at the edge of the core. Figure 4.1 (b) shows the voltage-time history at the inner edge of a core which corresponds with that shown in Figure 4.1 (b).

Table 4.1 lists both the initial circulation and the circulation measured at 7 De from the vortex generator exit for each test configuration used in the quantitative analysis. In general the results are in agreement with the slug model for ring circulation as the measurements show a clear increase in circulation with increasing stroke length. However the data display a wide variation in the degree of correspondence between initial ring circulation predicted by the slug model and measured circulation. Figure 4.2 is a plot of the ratio of measured circulation to initial circulation versus Reynolds number and shows that the more turbulent rings tended to loose more of their initial circulation. It is significant that the only truly laminar case, the straight tube configuration with a 0.25 inch stroke, is the ring which has lost the least circulation. These findings fit with the qualitative observations which indicated that for increasing Reynolds number the flow structure became more turbulent and that more dye (hence vorticity) was deposited into the ring's wake. In addition, the dye tests revealed that in comparison to the straight tube configuration, the sharp edged configuration with its higher exit velocities generated a more turbulent flow structure and rings which shed more vorticity. This also agrees with the quantitative results since the cases with the greatest decay in circulation were those generated by the sharp edged configuration.

Attempts were also made to measure the circulation of rings moving in a cross flow. Unfortunately the method which worked relatively well for rings in a quiescent tank proved extremely difficult to implement when a cross flow was added. The main difficulties were reliably locating the core of the vortex and accurately measuring velocity within the ring. An additional complication was that for cross flow, the ring's tilt angle had to be considered. The tilt angle was evaluated as shown in Figure 4.3 and required accurate identification of the core on both sides of the vortex ring. The horizontal distance was taken from the known distance between measurement stations 1 and 2 and the vertical

Table 4.1. Initial and measured ring circulation.

Configuration	Stroke (inches)	Γ_o (in^2/sec)	P- Piston Velocity Profile Correction Factor	Γ_m (in^2/sec)	$Re_M = \frac{\bar{U}_e D_e}{\nu}$
Sharp Edge - 75 psi	0.8	253.6	1.04	75.4	4.8×10^4
	0.5	126.1	1.02	43.3	3.7×10^4
	0.25	50.2	1.02	21.5	2.9×10^4
Straight Tube - 45 psi	0.8	19.0	1.55	9.1	1.4×10^4
	0.5	10.6	1.11	5.2	1.1×10^4
	0.25	3.9	1.19	3.0	7.9×10^3
Straight Tube - 45 psi $U_e/U_\infty = 14$ $\beta \approx 9^o$	0.25	3.9	1.19	0.7	7.9×10^3

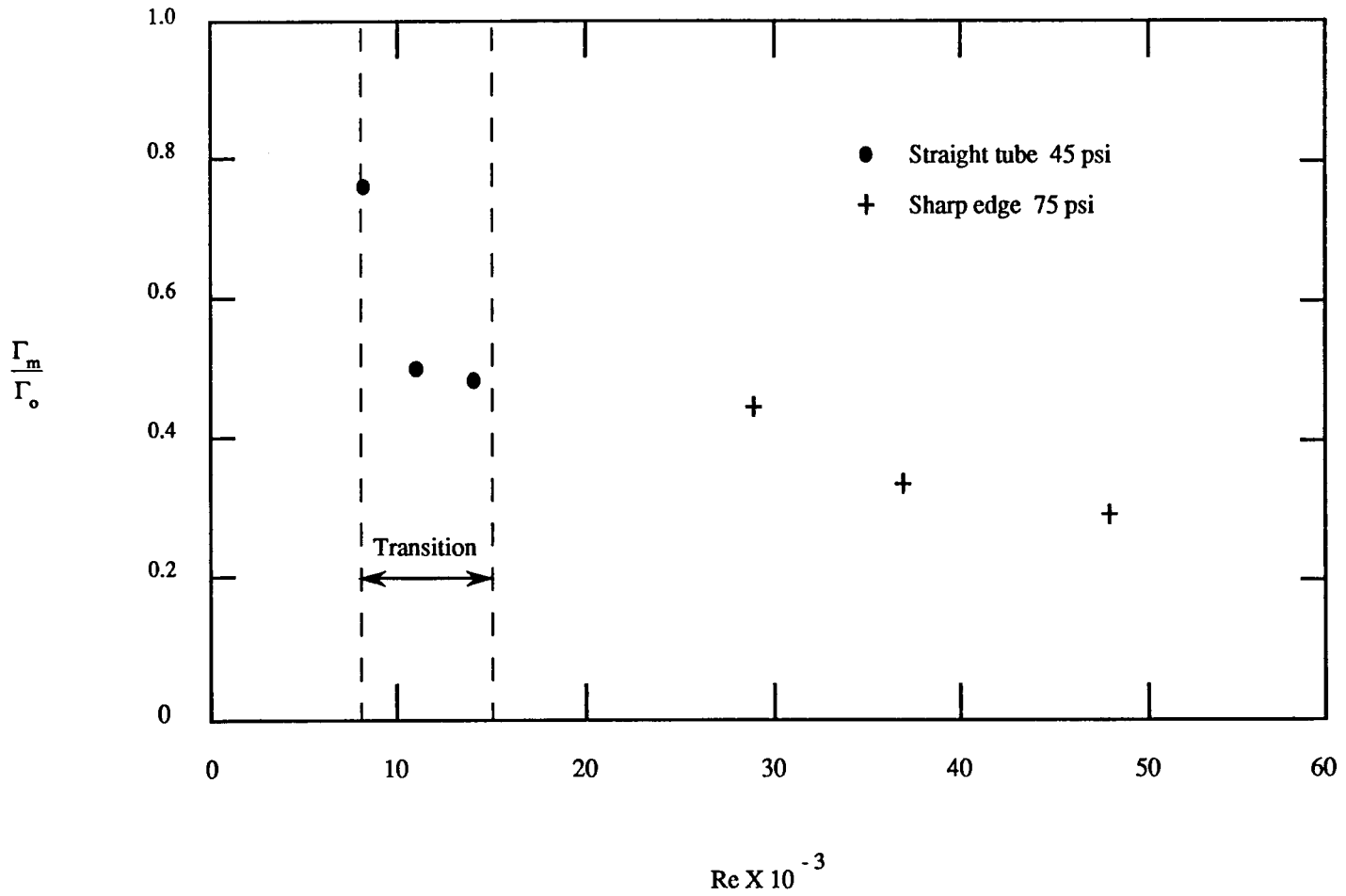


Figure 4.2. Ratio of measured to initial circulation versus Reynolds number.

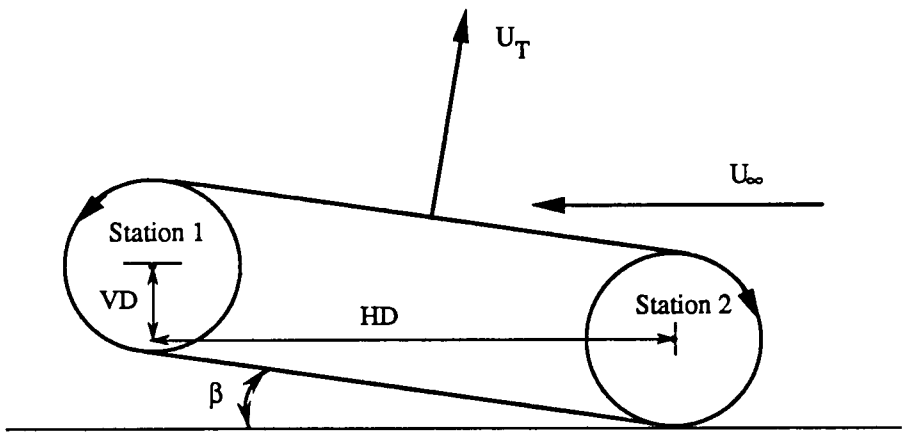


Figure 4.3. Measurement of vortex ring tilt angle.

relative time difference between stations 1 and 2 such that

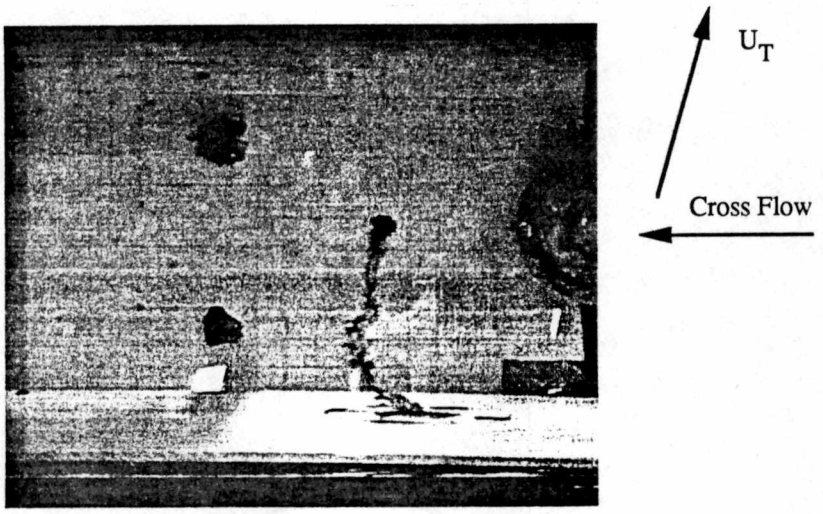
$$\beta = \tan^{-1} \frac{VD}{HD} . \tag{4.3}$$

In the end, only the slowest moving ring yielded a realistic measurement of circulation in a cross flow (included in Table 4.1), thus conclusions about the effects of a cross flow on ring circulation could not be drawn.

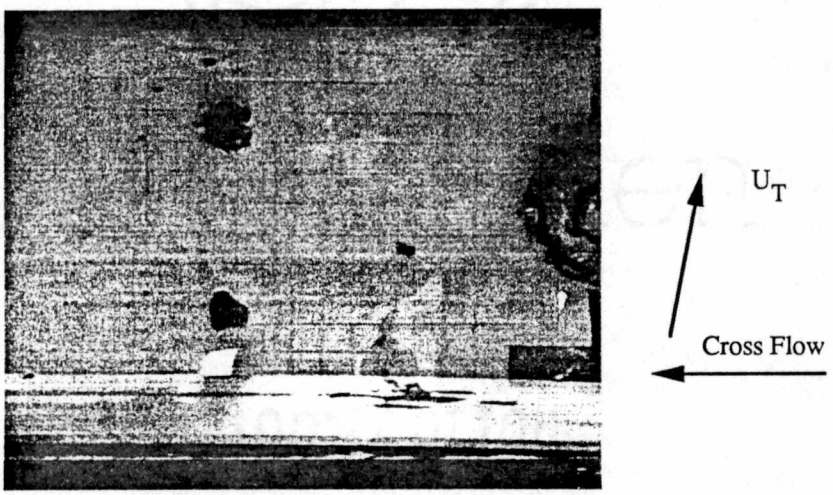
Returning to the tilt angle of a vortex ring in cross flow, because the tilt angle of the rings generated for the initial run of flow visualization tests was very small there was some doubt as to whether these ring actually tilted. Further investigation using rings with very weak vorticity and a low exit velocity to cross flow velocity ratio (U_e/U_∞) yielded conclusive evidence of the tilting of vortex rings in a cross flow. As shown by the examples included in Figure 4.4, by applying 35 to 25 psi to the straight tube piston-cylinder with a 0.25 inch stroke it was possible to generate rings which tilted as much as 10° to 20°. Interestingly, the ring wakes in Figure 4.4 are in effect trails which outline the ring trajectories; looking at the two trajectories it can be seen that they both had an upstream velocity component. This upstream velocity was simply the component of the rings' translational velocity which was directed upstream because of the rings' tilt angle. As U_e/U_∞ was further decreased the rings began to tilt during roll up. For extremely low values of U_e/U_∞ the incipient rings could be rotated a full 90°, however in these cases the cross flow destroyed the ring structure before it could fully form and quickly convected the remaining vorticity downstream.

Ring Diameter

Analysis of the flow visualization tests run to investigate overall ring diameter showed that for the straight tube configuration the diameter increased as the stroke length increased. As well, with the 0.5 and 0.25 inch strokes, for a given stroke it was possible to observe a slight decrease in ring diameter as higher exit velocities were used to generate the rings, but this effect was much less pronounced than the change in diameter with stroke length. It was also noted that the rings generated



(a) Straight tube - 0.25 inch stroke with 35 psi and $\frac{U_e}{U_\infty} = 9.2$



(b) Straight tube - 0.25 inch stroke with 25 psi and $\frac{U_e}{U_\infty} = 4.3$

Figure 4.4. Vortex rings tilting in a uniform cross flow.

with the straight tube, ranging from bordering on transition to mild turbulence, maintained their overall shape as they translated. For the range of U_e/U_∞ used for this set of experiments ($14 < U_e/U_\infty < 200$), the cross flow had no noticeable effect on ring diameter. However the above mentioned distortion of ring structure observed during the production of rings with large tilt angles suggests that for lower values of U_e/U_∞ the cross flow may have some effect on ring diameter.

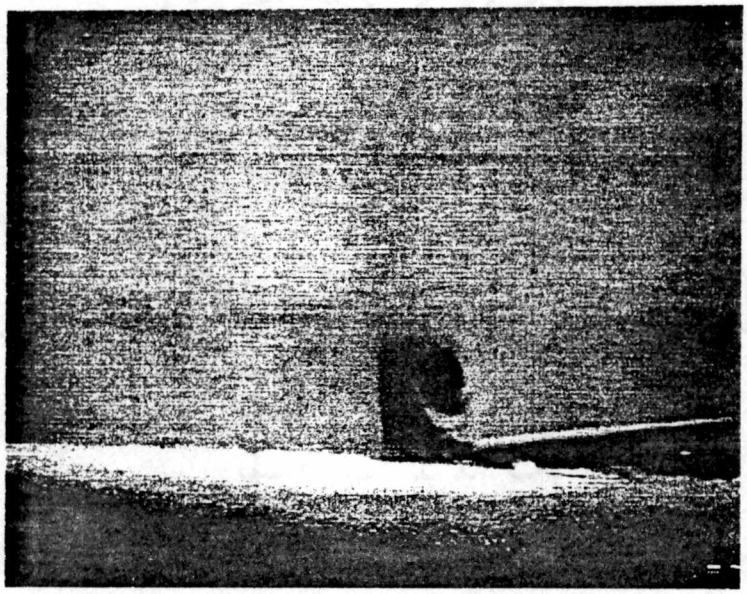
As with the straight tube, when the sharp edge was used the video tape showed that the ring diameter increased with stroke length. The sharp edged geometry also produced some distinctively different results. For most of the pressures used with the sharp edge and 0.25 inch stroke combination the rings behaved in much the same way as those generated with the straight tube, with the overall shape of the ring maintained as the diameter grew slowly. With higher pressures (75 and 85 psi) applied to the piston and higher exit velocities generated a change in the growth of the rings was noted. This change was noticeable after the rings had travelled roughly 15 D_e from the exit of the vortex generator and at this point the ring diameter increased greatly. Testing of the longer strokes showed that this rapid increase in ring growth occurred closer to the exit as stroke length increased. In addition, for a given stroke length there was some indication that this transition took place earlier as the exit velocity increased. In general, as Reynolds number increased this change tended to appear earlier and to be more noticeable. For very high Reynolds number an explosive increase in diameter, which ended with the ring's destruction, was observed. Another generalization was that the turbulent rings which displayed a rapid increase in growth did not maintain a constant overall shape. Finally, the cross flow did not have a visible effect on the diameter of the sharp edged rings.

Entrainment

The flow visualization tests run to investigate entrainment during the formation of a vortex ring yielded some good footage of how the slug of fluid from the cylinder incorporated fluid from the region around the generator orifice into the ring structure during roll up thus giving insight into how ring diameter and entrainment differed for the various configurations tested. Figure 4.5 presents two



(b) Fluid 1 to 2 De from the exit



(a) Fluid emerging from the cylinder

Figure 4.5. Flow visualization results of entrainment process.

digitized reproductions of the video taped results. Figure 4.5 (a) shows that as the undyed slug emerged from the cylinder, the dye which was distributed around the orifice was quickly pulled into the forming ring. In Figure 4.5 (b) the fluid has moved 1 D_e to 2 D_e from the exit.

Since the digitized pictures of Figure 4.5 do not clearly show all of the features which were visible on the video tape, Figure 4.6 has been included to illustrate the case of the straight tube configuration operated with a stroke length of 0.8 inches and at 55 psi. It shows that the dye streaklines outlined the vortical structure of the ring and that a solid disc of dye was visible at the centre of the core. Although care was taken to distribute the dye along an arc which was less than one half of the generator's exit circumference, the results showed traces of dye on the opposite side of the ring. This would seem to indicate the presence of an azimuthal velocity within the ring. This observation held for almost all of the rings generated for this entrainment experiment and as all of the rings were either at the upper end of the laminar range, in transition or turbulent, this result is in agreement with researchers such as Maxworthy (8) who found that an azimuthal velocity is initiated during transition.

An exit velocity which was twice as fast as that for the 55 psi test was obtained by applying 85 psi to the straight tube and 0.8 inch stroke combination. The results for this case were very similar to those for the slower ring except that the concentration of dye throughout the ring was weaker and in particular the streaklines were fainter. This suggests that the slower moving ring entrained more fluid from the exit area, however it should be noted that while care was taken to deposit equal concentrations of dye outside the orifice for each test, this part of the procedure was not precisely regulated. Additionally, while the piston velocity profiles used to generate the two rings were of the same general shape, they were not exactly similar.

In order to provide a comparison of the two different exit geometries the tests were repeated using the sharp edged piston with a 0.8 inch stroke. The 25 psi and 45 psi tests had roughly the same exit velocity, respectively, as the 55 psi and 85 psi straight tube configurations. Once again the piston

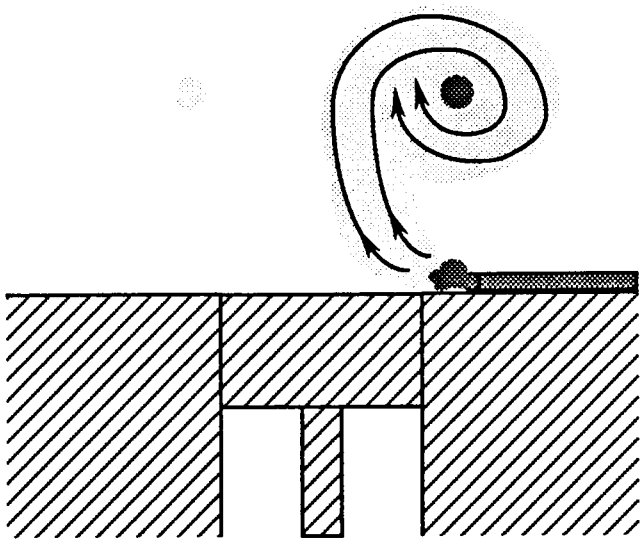


Figure 4.6. Flow visualization of straight tube vortex ring entrainment properties.

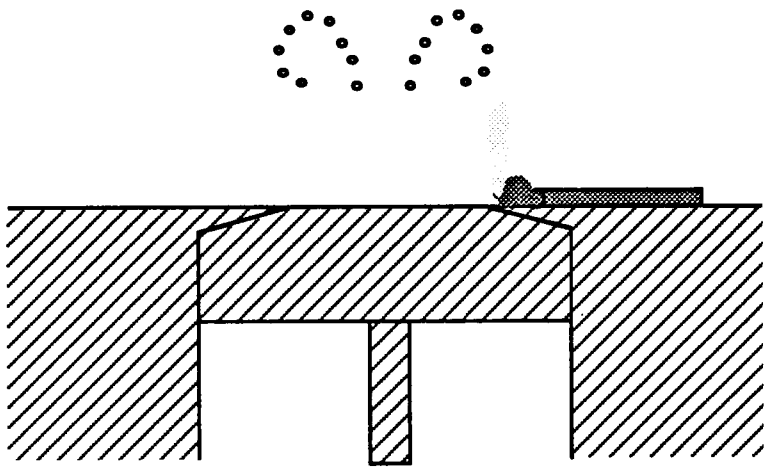
velocity profiles were not exactly similar. The slow ring created with the sharp edge had a smaller diameter and entrained less fluid from the exit area than its straight tube counterpart. As shown in Figure 4.7 (a), this ring entrained very little fluid, it contained extremely weak concentrations of dye and no streaklines were visible. The faster sharp edged ring entrained almost no dye and as a consequence this ring was very difficult to identify. Fortunately air bubbles which were in the cylinder cavity reflected enough light to make the ring visible. Figure 4.7 (b) shows that this very fast moving ring appeared to rush past the dye outside the orifice incorporating no dye into the ring structure and pulling only faint traces of dye into its wake.

Core Diameter

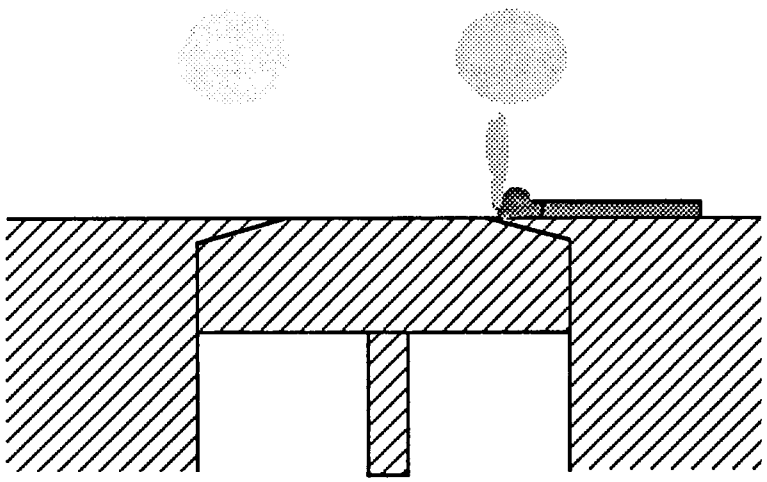
The core measurements indicate a tendency for the core diameter to increase slightly with both stroke length and Reynolds number, but, the results did not display a clear relationship between core diameter and either of these two parameters. On the other hand, the results do clearly show that the cores of the rings generated with the sharp edged geometry were significantly larger than the cores of rings produced with the straight tube. The data suggests a correspondence between the increase in core diameter and the increase in the cross sectional area of the cylinder used in the vortex generator. However this relationship would have to be investigated further before a firm conclusion could be drawn.

Translational Velocity

This study did not directly explore possible connections between piston stroke length or exit geometry and vortex ring translational velocity. Translational velocity was measured only for the purpose of evaluating ring circulation.



(a) 45 psi test



(a) 25 psi test

Figure 4.7. Flow visualization of sharp edge vortex ring entrainment properties.

Accuracy of Experimental Results

Since circulation and core diameter were evaluated based on measurements it is possible to estimate the level of uncertainty in the experimental results for these two characteristics. Chang (10) listed the uncertainties inherent in taking hot film measurements with the experimental set up used for this study, these are presented in Table 4.2.

Table 4.2. Uncertainties in hot film measurements.

Source of Uncertainty	Uncertainty
Calibration constants (A and B)	± 4 %
Probe position in streamwise direction	± 0.0052 inches
Probe position in vertical direction	± 0.0052 inches
Probe position in spanwise direction	± 0.0100 inches
Angular position of probe	± 2.5 °

According to Kline and McClintock (18), the uncertainty in a value calculated from experimental measurements can be expressed as

$$\Delta Q = \left[\left(\frac{\partial Q}{\partial G_1}\Delta G_1\right)^2 + \left(\frac{\partial Q}{\partial G_2}\Delta G_2\right)^2 + ... + \left(\frac{\partial Q}{\partial G_n}\Delta G_n\right)^2\right]^{\frac{1}{2}} \tag{4.4}$$

where

$$Q = Q(G_1, G_2, ... G_n,) . \tag{4-5}$$

Chang (10) used this approach to estimate that, for velocities typical of those encountered in this study, the uncertainty in the evaluation of the vertical velocity component ($\bar{W}$) was 0.06 in/sec. Since the vertical velocity component is used to determine velocities within the vortex ring, it is

assumed that this level of uncertainty applies to both the translational velocity of the ring and the rotational velocity at the edge of the core.

Assuming that there is negligible uncertainty in the measurement of time, the uncertainty in evaluating core diameter as per equation (4.1) is expressed in terms of equation (4.4), by Schenck (19), as

$$\frac{\Delta d}{d} = \frac{\Delta U_T}{U_T} . \tag{4.6}$$

Using equation (4.6), the maximum uncertainty in the evaluation of core diameter for these experiments was 5 %.

Again applying equation (4.4), the uncertainty in the measurement of total ring circulation is

$$\frac{\Delta \Gamma_m}{\Gamma_m} = \left[\left(\frac{\Delta U_{rot}}{U_{rot}} \right)^2 + \left(\frac{\Delta d}{d} \right)^2 \right]^{\frac{1}{2}} . \tag{4.7}$$

Using equation (4.7), the uncertainty in the measurement of ring circulation was estimated to be less than 7.5 %.

CHAPTER V
CONCLUSIONS AND RECOMMENDATIONS

This study was conducted in order to investigate the links between the piston stroke length and exit geometry of a vortex generator and the dependent characteristics of a vortex ring. Based on the investigation, the following conclusions can be drawn:

1) Using hot film anemometer measurements it was confirmed that, within the range of parameters studied, increasing the piston stroke length of the vortex generator resulted in an increased ring circulation;

2) Flow visualization results also confirmed that ring diameter increased with increasing stroke length;

3) Flow visualization revealed that when highly turbulent rings were produced they underwent a rapid increase in ring growth after travelling 10 to 15 D_e from the vortex generator. This change occurred earlier as stroke length and Reynolds number increased. While these rings became unstable and did not maintain their overall shape, rings which did not undergo transition did;

4) Both measurements and flow visualization results demonstrated that as Reynolds number increased a greater percentage of the ring's initial circulation was shed into its wake. The rings which experienced the greatest loss of vorticity were those produced by the sharp edged configuration, these rings tended to be more turbulent because of the high exit velocities associated with this geometry;

5) The entrainment tests confirmed that rings produced with the sharp edged geometry entrained less fluid from the exit area of the vortex generator than those generated with the straight tube. As well, for a given configuration the slower moving rings entrained more fluid;

6) The entrainment tests provided evidence that the sharp edged rings had smaller diameters than their straight tube counterparts and hot film measurements indicated that the cores of the sharp edged rings were larger; and

7) Using flow visualization it was possible to clearly show that for low values of U_e/U_∞ vortex rings in a cross flow did in fact tilt.

A number of recommendations can also be made based on the finding of this study:

1) Further work on the procedure for taking hot film measurements of a vortex rings in a cross flow is required. The feasibility of using Sallet and Widmayer's (15) three probe array should be investigated;

2) Flow measurements should be used to follow up on the flow visualization results which suggested that higher exit velocities resulted in rings with smaller overall diameters and hence less diffusion of vorticity; and

3) Finally, experiments should be conducted using a lower range of U_e/U_∞ in order to explore the effects that cross flow may have on ring diameter.

LIST OF REFERENCES

LIST OF REFERENCES

1. Vakili, A.D., Chang,Y.K., and Wu, J.M., "Vortex Rings in Uniform Cross-Flow," Presented at AIAA 29th Aerospace Sciences Meeting, AIAA Paper 91-0522, Reno, Jan. 1991.
2. Vakili, A.D., "Review of Vortical Flow Utilization," Presented at AIAA 16th Aerodynamic Ground Testing Conference, AIAA Paper 90-1429, Seattle, June 1990.
3. Didden, N., "On the Formation of Vortex Rings: Rolling Up and Production of Circulation," Journal of Applied Mathematics and Physics, Vol. 30, 1979, pp. 101-106.
4. Batchelor, G.K., An Introduction to Fluid Dynamics, Cambridge University Press, 1967.
5. Magarvey, R.H. and MacLatchy, C.S., "The Formation and Structure of Vortex Rings," The Canadian Journal of Physics, Vol. 42, April 1964, pp. 678-683.
6. Maxworthy, T., "The Structure and Stability of Vortex Rings," Journal of Fluid Mechanics, Vol. 51, Part 1, 1972, pp. 15-32.
7. Maxworthy, T., "Turbulent Vortex Rings," Journal of Fluid Mechanics, Vol. 64, Part 2, 1974, pp. 227-239.
8. Maxworthy, T., "Some Experimental Studies of Vortex Rings," Journal of Fluid Mechanics, Vol. 81, Part 3, 1977, pp. 465-495.
9. Glezer, A., "The Formation of Vortex Rings," The Physics of Fluids, Vol.31, No. 12, December 1988, pp. 3532-3542.
10. Chang, Y.K., "Dynamics of Vortex Rings in Cross Flow," UTSI Dissertation, Dec. 1991.
11. Lamb, H., Hydrodynamics, Dover Publications, 1945.
12. Sallet, D.W., and Widmayer R.S., "An Experimental Investigation of Laminar and Turbulent Vortex Rings in Air," Z. Flugwiss., Vol. 22, 1974, pp. 207-215.
13. Saffman, P.G., "The Velocity of Viscous Vortex Rings," Studies in Applied Mathematics, Vol. 49, No. 4, Dec. 1970, pp. 371-379.

14. Caruthers, J., Ma, H.Y., and Wu, J.Z., "A Note on the Kutta-Joukowski Formula," Developments in Theoretical and Applied Mathematics, Vol. XVI, The University of Tennessee Space Institute, 1992, pp. II.14.43-51.

15. Fingerson, L.M., and Freymuth, P., "Thermal Anemometers," in IFA 100 System Instruction Manual, TSI, 1983.

16. Jorgensen, F.E., "Directional Sensitivity of Wire and Fiber-Film Probes," DISA Information No. 11, May 1971, pp. 31-37.

17. Hinze, J.O., Turbulence, McGraw-Hill, 1959.

18. Kline, S.J., and McClintock, F.A., "Describing Uncertainties in Single-Sample Experiments," Mechanical Engineering, Jan. 1953, pp. 3-8.

19. Schenck, H., Theories of Engineering Experimentation, McGraw-Hill, 1961.

APPENDICES

APPENDIX A
DIMEMSIONAL ANALYSIS FOR INITIAL VORTEX RING CIRCULATION

For a general case the relationship between initial ring circulation and the independent parameters can be described by the following function

$$f_1\left(\Gamma_o, L_p, D_e, D_p, \overline{U_p^2}, T_o, \mu_1, \rho_1, T_1, R_g, C_{po}\right) = 0. \tag{A-1}$$

This representation assumes a pefect gas. Additionally, for gases, the piston motion may result in significant changes in the density of the fluid within the cylinder, for this reason, the function (A-1) takes compressibility effects into consideration.

Dimensional analysis results in

$$f_2\left(\frac{\Gamma_o T_o}{L_p^2}, \frac{L_p}{D_p}, \frac{D_e}{D_p}, \overline{U_p^2}\left[\frac{T_o}{L_p}\right]^2, \frac{\rho_1 \frac{L_p}{T_o} D_e}{\mu_1}, \gamma, \frac{\frac{L_p}{T_o}}{\sqrt{\gamma R_g T_1}}\right) = 0. \tag{A-2}$$

However

$$\frac{L_p}{T_o} = \overline{U_p} \tag{A-3}$$

and

$$P = \frac{\overline{U_p^2}}{\overline{U_p}^2}, \tag{A-4}$$

thus (A-2) can be reduced to

$$f_3\left(\frac{\Gamma_o T_o}{L_p^2}, \frac{L_p}{D_p}, \frac{D_e}{D_p}, P, Re_1, \gamma, M_1\right) = 0. \tag{A-5}$$

Where P is the velocity profile correction factor which, as discussed in chapter II, can be used to account for deviations from a constant piston velocity profile. For an incompressible fluid with weak dependence on Reynolds number, this simply reduces to

$$f_4\left(\frac{\Gamma_o T_o}{L_p^2}, \frac{L_p}{D_p}, \frac{D_e}{D_p}, P\right) = 0. \tag{A-6}$$

APPENDIX B

LOWER BOUND OF PISTON VELOCITY PROFILE CORRECTION FACTOR

The Schwarz integral inequality

$$\left(\int_a^b x(t)\, y(t)\, dt\right)^2 \le \int_a^b x^2(t)\, dt \int_a^b y^2(t)\, dt \tag{B-1}$$

can be used to show that the piston velocity profile correction factor of equation (2.11) has a lower bound such that $P \ge 1$.

For $P \ge 1$,

$$\overline{U_p}^2 \le \overline{U_p^2} \tag{B-2}$$

where

$$\overline{U_p^2} = \frac{1}{T_o}\int_0^{T_o} U_p^2(t)\, dt \tag{B-3}$$

and

$$\overline{U_p}^2 = \frac{1}{T_o^2}\left(\int_0^{T_o} U_p^2(t)\, dt\right)^2. \tag{B-4}$$

In the inequality (B-1) let $x(t) = U_p(t)$ and $y(t) = 1$. Now (B-1) can be written as

$$\left(\int_0^{T_o} U_p(t)\, dt\right)^2 \le \int_0^{T_o} U_p^2(t)\, dt \int_0^{T_o} dt \tag{B-5}$$

$$\left(\int_0^{T_o} U_p(t)\, dt\right)^2 \le T_o \int_0^{T_o} U_p^2(t)\, dt \tag{B-6}$$

dividing by T_o^2

$$\frac{1}{T_o^2}\left(\int_0^{T_o} U_p(t)\, dt\right)^2 \le \frac{1}{T_o}\int_0^{T_o} U_p^2(t)\, dt\,. \tag{B-7}$$

With $\overline{U_p^2}$ and $\overline{U_p}^2$ defined by (B-3) and (B-4), (B-10) confirms that $P \ge 1$.

VITA

Andrew Stewart Fleming was born on 29 July 1964 in Toronto, Canada. He entered the Mechanical Engineering program at the University of Toronto in 1983. During his studies he enrolled in the Canadian Forces Regular Officer Training Program and upon graduation from the University of Toronto he was commissioned as an officer in the Canadian Forces.

After graduation he worked, in Ottawa, on the maintenance and engineering program for the DeHavilland Dash 8 aircraft operated by the Canadian Forces. He came to the University of Tennessee Space Institute in August 1990 and graduated with a Master of Science Degree in Aerospace Engineering in August 1992.